Large-scale (in) stability analysis of an exactly solved coupled dark-energy model

Weiqiang Yang,[1,*] Supriya Pan,[2,†] Ramón Herrera,[3,‡] and Subenoy Chakraborty[4,§]

[1]*Department of Physics, Liaoning Normal University, Dalian 116029, P. R. China*
[2]*Department of Mathematics, Raiganj Surendranath Mahavidyalaya, Sudarsharpur, Raiganj, Uttar Dinajpur, West Bengal 733134, India*
[3]*Instituto de Física, Pontificia Universidad Católica de Valparaíso, Casilla 4059, Valparaíso, Chile*
[4]*Department of Mathematics, Jadavpur University, Kolkata, West Bengal 700032, India*

(Received 23 March 2018; published 15 August 2018)

Assuming a nongravitational interaction among the dark fluids of our Universe—namely, dark matter and dark energy—we study a specific interaction model in the background of a spatially flat Friedmann-Lemaître-Robertson-Walker geometry. We find that the interaction model solves the background evolution in an analytic way when the dark energy takes a constant barotropic equation of state, w_x. In particular, we analyze two separate interaction scenarios, namely, when the dark energy is a fluid other than the vacuum energy (i.e., $w_x \neq -1$) and when it is vacuum energy itself (i.e., $w_x = -1$). We find that the interacting model with $w_x \neq -1$ produces stable perturbations at large scales for $w_x < -1$ with the coupling strength $\xi < 0$. Both scenarios are constrained by the latest astronomical data. The analyses show that a very small interaction with the coupling strength is allowed, and within the 68.3% confidence region $\xi = 0$ is recovered. The analyses further show that a large coupling strength significantly affects the large-scale dynamics of the Universe, while according to the observational data the interaction models are very well consistent with Λ cosmology. Furthermore, we observe that for the vacuum interaction scenario, the tension on H_0 is not released while for the interacting dark energy scenario with $w_x < -1$, the tension on H_0 seems to be released partially because of the high error bars in H_0. Finally, we conclude the work by calculating the Bayesian evidence, which shows that ΛCDM cosmology is favored over the two interacting scenarios.

DOI: 10.1103/PhysRevD.98.043517

I. INTRODUCTION

The theory of nongravitational interactions between dark matter and dark energy is the main concern of this work. The origin of such an interacting theory did not appear suddenly in the cosmological scheme. It has a well-motivated history that we shall discuss here. However, before that, we need a basic introduction about dark matter and dark energy. According to the latest observational suggestions [1], dark matter (DM) and dark energy (DE) are the main influential sources of the total energy budget of the Universe, where dark matter contributes around 26% of its total energy density, is pressureless, and unseen, while dark energy—a hypothetical fluid making up 68% of the total energy density of the Universe—is accelerating the expansion history of the Universe. The best description for such observational information is ΛCDM cosmology, where Λ acts as the dark energy fluid and cold dark matter (CDM) is pressureless. This is a noninteracting scenario in the sense that both Λ and CDM are separately conserved. Despite the great success of ΛCDM cosmology, the cosmological constant problem [2] still lacks a satisfactory explanation. The cosmological constant problem refers to the mismatched value of the cosmological constant predicted from the high- and low-energy scales of the Universe. In the following, we shall discuss how the interacting dynamics is closely related to the cosmological constant problem. In fact, this coupling mechanics was developed because of the cosmological constant problem, and it became very useful for explaining some other issues. We now give a detailed discussion on the origin of interacting dark matter and dark energy.

In the late 1980s there was no concept of dark energy, but the discrepancy in Λ was still a serious issue for modern cosmology. To account for this issue, one of the attempts was to consider a toy model where a scalar field is coupled to gravity [3]. The energy-momentum tensor of such a coupled scalar field introduces a time-dependent cosmological constant and, consequently, it became a possible solution to the cosmological constant problem since the issue regarding the time-independent cosmological constant is naturally solved due to the variable nature of the

*d11102004@163.com
†span@research.jdvu.ac.in
‡ramon.herrera@pucv.cl
§schakraborty@math.jdvu.ac.in

cosmological constant. After the official introduction of dynamical dark energy models in several forms (see Refs. [4–6] for a detailed survey), it was found that they automatically induce the coincidence problem [7]. We note that the cosmological constant being time-independent cannot escape from the same problem. Quite interestingly, it was reported in Ref. [8] that if dark energy and dark matter are allowed to interact nongravitationally with each other, the coincidence problem can be solved. Following this, a series of works with coupled dark matter and dark energy had the same conclusions [9–13]. However, some recent results have fueled the investigations of coupled dark matter and dark energy with the claim that the observational data favor an interaction in the dark sector [14–23]. Additionally, some very recent investigations in this direction strongly claim that the tension on the local Hubble constant can be released if the interaction in the dark sector is allowed.

However, the most important question in the coupling dynamics is, what is the appropriate energy transfer rate between the dark sectors? Before we look for an appropriate transfer rate, we recall that the nature of both dark matter and dark energy is unknown. Thus, the sensible approach is to consider some well-motivated phenomenological transfer rates or interaction functions and test the expansion history with the available astronomical data. A number of different interaction rates between dark matter and dark energy have been studied in the last several years [24–56]. For a comprehensive review on different interaction rates, we refer to Refs. [57,58]. We also note that the interaction between the dark sectors has also been examined in a more general framework where the geometry of the Universe is inhomogeneous [59,60].

In this work we concentrate on the spatially flat Friedmann-Lemaître-Robertson-Walker universe where we introduce an interaction between dark energy and pressureless dark matter that exactly solves the background evolution. This means that the evolution equations for dark matter and dark energy are analytically solved. The appearance of an analytic structure for the background evolution makes the cosmological model quite interesting because the cosmological parameters associated with this model take analytic forms too. However, this is not new because the analytic structure for such an interaction model has already been reported by some of the authors in a previous work [61]. But the motivation of the present work is completely different. Here, we aim to test the large-scale stability of the model which is very important because without stable perturbations there will be no such structure formation in the Universe.

The analysis of structure formation in models of DE and DM, from the point of view of cosmological perturbation theory, plays an essential role when the different models are confronted with observational data [62]. As is well known, these dark scenarios imprint a signature on the cosmic microwave background (CMB) power spectrum [63,64]. Thus, the study of the cosmological perturbations is important and also requires thorough analysis. In particular, models with interactions between DE and DM with adiabatic initial conditions and perturbation theory were studied in Ref. [65,66]; see also Refs. [58,67,68]. Also, models with DE-DM interactions with a constant equation of state were analyzed in Ref. [69]. There, the authors demonstrated that perturbations were unstable due to a rapid growth of DE fluctuations. In this sense, testing large-scale stability is fundamental, since without stable perturbations there will be no such structure formation.

We organize the work in the following way. In Sec. II we describe the basic equations for the interacting model at both the background and perturbative levels. The analytical solutions are discussed in Sec. III. Section V details the results of the analysis following the observational data used in this work. Finally, we close our work with a brief summary in Sec. VI.

II. INTERACTING DYNAMICS IN FLAT FLRW

We consider a spatially flat Friedmann-Lemaître-Robertson-Walker (FLRW) universe where pressureless dark matter, also known as cold dark matter, interacts with a dark energy fluid. The interaction is nongravitational, which means that gravity does not play any role in their interaction. Additionally, we consider the existence of baryons and radiation in the universe sector. To avoid any kinds of inflexible constraints like a "fifth force," we assume that neither baryons nor radiation takes part in the interaction. In other words, they are separately conserved. Since the interaction exists between CDM and DE, the total conservation of this (CDM + DE) sector is

$$\dot{\rho}_c + 3H(1+w_c)\rho_c = -\dot{\rho}_x - 3H(1+w_x)\rho_x, \quad (1)$$

where (ρ_c, ρ_x) are, respectively, the energy density of CDM and DE. The parameter $H \equiv \dot{a}/a$ corresponds to the Hubble rate, with a being the FLRW scale factor. The quantity $w_x = p_x/\rho_x$ corresponds to the equation of state for DE and p_x is the pressure of the DE fluid. Also, we note that $w_c = p_c/\rho_c$ since p_c (the pressure of CDM) is zero, and hence $w_c = 0$. The total conservation equation (1) can be decoupled into the following equations:

$$\dot{\rho}_c + 3H\rho_c = -Q, \quad (2)$$

$$\dot{\rho}_x + 3H(1+w_x)\rho_x = Q, \quad (3)$$

where an overdot represents differentiation with respect to cosmic time. The parameter Q denotes the energy transfer between the dark sectors. In this sense, the sign of Q determines the direction of energy transfer. For instance, $Q < 0$ indicates energy transfer from dark energy to CDM, while $Q > 0$ means the energy flow occurs from CDM

to DE. In terms of the Hubble parameter H, we have the following constraint or Friedmann equation:

$$H^2 = \frac{8\pi G}{3}(\rho_r + \rho_b + \rho_c + \rho_x). \tag{4}$$

Thus, the dynamical evolution of the universe can be determined from Eqs. (2)–(4) once the interaction rate Q is specified.

Introducing $\rho_t = \rho_c + \rho_x$ as the total energy density of the dark sector, one can express the energy densities for dark energy and dark matter, respectively, as

$$\rho_x = -\left(\frac{\rho_t' + 3\rho_t}{3w_x}\right), \tag{5}$$

$$\rho_c = \left(\frac{\rho_t' + 3(1+w_x)\rho_t}{3w_x}\right), \tag{6}$$

where the prime stands for differentiation with respect to the lapse function $N = \ln(a/a_0) = \ln a$ (here, we set a_0—the present day value of the scale factor—to unity). Now, by inserting Eq. (5) into Eq. (3) or Eq. (6) into Eq. (2) we find that the differential equation for the total energy density of the dark sector is given by

$$\rho_t'' + 3\left[2 + w_x - \frac{w_x'}{3w_x}\right]\rho_t' + 9\left[(1+w_x) - \frac{w_x'}{3w_x}\right]\rho_t = -3\bar{Q}w_x, \tag{7}$$

where $\bar{Q} = Q/H$. Given the interaction Q and the equation of state w_x, the differential equation (7), if solved, can determine the evolution of each dark sector separately which can be obtained from Eqs. (5) and (6). In this context, because both dark components are assumed to interact with each other, we must define the interaction rate Q in order to obtain analytical solutions. As we mentioned before, different expressions have been considered in the literature for the interaction rate Q. The most commonly studied energy transfer between the dark sectors depends on the energy densities (ρ_x, ρ_c, ρ_t) or some combinations of these, multiplied by a quantity with units of inverse time, which could be a rate or a differentiation with respect to time. Commonly, this rate corresponds to the Hubble rate. In particular, in the reheating scenario this rate was considered as a constant [70], and an analogous situation for the curvaton field case was considered as well [71]. In the following, we will consider that the transfer rate Q is proportional to the Hubble rate, as discussed above. Thus, we have

$$Q = -\xi(\dot{\rho}_c + \dot{\rho}_x) = -\xi\dot{\rho}_t, \tag{8}$$

where ξ is the coupling parameter of the interaction characterizing the strength and direction of energy transfer between the dark sectors. We note that the negative sign before the coupling parameter in Eq. (8) is not related to the physics of dark matter and dark energy interactions. The typical choice of the interaction (8) is actually motivated by phenomenology, together with the fact that the background energy conservation equations are easily solved. In this sense, other interaction rates in the literature have been studied, such as $Q \propto \rho_c$ [32], $Q \propto \rho_x$ [33], $Q \propto (\rho_c + \rho_x)$ [31], $Q \propto (\rho_c\rho_x)$ [30], $Q \propto (\rho_x\rho_c)(\rho_c + \rho_x)^{-1}$ [44], $Q \propto \rho_x^2/\rho_c$ [21], and $Q \propto \dot{\rho}_x$ [23] (also see Ref. [57] for some other interaction models). We also mention that the evolution of an inhomogeneous mixture of nonrelativistic pressureless CDM coupled to DE in which the interaction term is proportional to the DE density was studied in Ref. [60]. There, from the spherically symmetric Lemaître-Tolman-Bondi metric, the authors found that the interaction Q can be written as $Q \propto \dot{\rho}_x$ (as in Ref. [23]). In this sense, from Eq. (8) the presence of $\dot{\rho}_t$ creates some differences from the usual and well-known interaction models. Looking at Eq. (8), one can understand that for positive coupling parameter ($\xi > 0$) the interaction rate could be positive, i.e., $Q > 0$ (energy flows from CDM to DE) if $\dot{\rho}_t < 0$, which means that the total energy density of the dark fluids decreases with the evolution of the universe. On the other hand, the interaction rate could be negative, i.e., $Q < 0$ (energy flows from DE to CDM) if $\dot{\rho}_t > 0$, which means that the total energy density of the dark fluids increases with the evolution of the universe. Similarly, for $\xi < 0$, one also encounters the following two possibilities: the interaction rate is positive (i.e., $Q > 0$) for $\dot{\rho}_t > 0$ and it is negative (i.e., $Q < 0$) for $\dot{\rho}_t < 0$. Thus, one can see that the flow of energy between the dark sectors is not only governed by the sign of the coupling parameter, but it also depends on the evolution of the total dark fluid. This might be considered to be an interesting property of the present interaction since in most of the usual interaction models the direction of energy flow is actually determined only from the coupling parameter. The interaction (8) was explicitly studied in Ref. [42] where the particular case of an interaction between the cosmological constant and matter was considered. However, a careful survey of the literature shows the existence of this interaction in Ref. [30], much earlier than Ref. [42].

Subsequently, using the same interaction, the background evolution of the universe was investigated in a generalized way where the dark energy equation of state was considered to be either constant or variable [61]. However, no such perturbation analysis was performed for this interaction and this analysis is an essential issue related to the structure formation of the Universe. We also observe another interesting feature in this interaction and we believe this is worth further investigations. In order to understand this feature we can rewrite Eq. (8) in a different way, which can be found using the conservation

equations (2) and (3) where the rate precisely corresponds to the Hubble parameter, such that

$$Q = 3\xi H[\rho_c + (1 + w_x)\rho_x]. \tag{9}$$

One can now notice that the interaction (9) includes the dark energy equation of state w_x aside from the coupling parameter. This differs from the well-known interactions where only the energy densities are considered. The incorporation of the energy transfer $Q \propto \dot{\rho}_t$ and hence the inclusion of the equation of state could result in a noninteracting scenario (equivalently, $Q = 0$) even if the coupling parameter is nonzero. In other words, for $w_x = -1 - \rho_c/\rho_x = -1 - r < -1$, where $r = \rho_c/\rho_x > 0$ is the coincidence parameter, the noninteracting physics is still realized even for $\xi \neq 0$. We call this the "*zero-coupling condition*." This kind of interaction—which retrieves the noninteraction cosmology with some nonzero coupling strength—is rare in the literature. We further notice that the dark energy equation of state in this case belongs to the phantom regime. We admit that the physics of this zero-coupling condition is very strange at least at the present stage, and it surely deserves further investigations. We note that a more general interaction scenario recovering the above interaction (8) [or Eq. (9)] was first introduced in Ref. [30] and recently in Ref. [53], where the authors discussed the analytical solutions for dark matter and dark energy. Certainly, a general interaction recovering different interaction rates as special cases would include a large number of coupling parameters. The stability of such a general interaction model is surely interesting; however, in this work we focus only on the stability of the simplest interaction model that offers an analytic structure.

III. EXACT SOLUTIONS

The differential equation (10) is the main tool to understand the evolution of the dark sector, provided it is exactly solved. For a constant dark energy equation of state, the differential equation (10) is simplified to

$$\rho_t'' + 3[2 + w_x]\rho_t' + 9[1 + w_x]\rho_t = -3\bar{Q}w_x = 3\xi w_x \rho_t', \tag{10}$$

and with the use of the interaction (8) the auxiliary equation becomes $m^2 + 3(2 + w_x - \xi w_x)m + 9(1 + w_x) = 0$. Now, under the condition $\Delta > 0$ where Δ is the discriminant of the above auxiliary equation, the exact solution of the above differential equation is

$$\rho_t = \rho_1 a^{m_1} + \rho_2 a^{m_2}, \tag{11}$$

where ρ_1, ρ_2 are the constants of integration. The integration constants must be positive; otherwise, if one of them is negative, then at some finite scale factor $\rho_t \equiv 0 \Rightarrow 3H^2 \approx \rho_b + \rho_r$, which means that the evolution of the Universe is governed by the baryons and radiation, which is purely unphysical from the available observational data. Thus, we shall strictly assume that $\rho_1 > 0$ and $\rho_2 > 0$. The roots of the auxiliary equation (m_1, m_2) are given by

$$m_1 = \frac{3}{2}[-(2 + w_x - \xi w_x) + \sqrt{\Delta}], \tag{12}$$

$$m_2 = \frac{3}{2}[-(2 + w_x - \xi w_x) - \sqrt{\Delta}], \tag{13}$$

where $\Delta = (1 - \xi)^2 w_x^2 - 4\xi w_x$. In particular, for the case in which $|\xi| \ll 1$ and as $|w_x| \sim \mathcal{O}(1)$, we have $\Delta \sim w_x^2 > 0$. In this sense, for $\Delta > 0$, the exact evolution equations for dark energy and cold dark matter become

$$\rho_x = -\left(\frac{1}{3w_x}\right)[\rho_1(m_1 + 3)(1 + z)^{-m_1} + \rho_2(m_2 + 3)(1 + z)^{-m_2}], \tag{14}$$

$$\rho_c = \left(\frac{1}{3w_x}\right)[\rho_1(m_1 + 3 + 3w_x)(1 + z)^{-m_1} + \rho_2(m_2 + 3 + 3w_x)(1 + z)^{-m_2}], \tag{15}$$

where $1 + z = a_0 a^{-1} = a^{-1}$ (since we have set $a_0 = 1$). Using the present-day values of the cosmological parameters, the evolution equations for dark energy and dark matter can be recast, respectively, as

$$\rho_x = -\left(\frac{1}{3w_x}\right)\left[\left(\frac{(m_2 + 3 + 3w_x)\rho_{x,0} + (m_2 + 3)\rho_{c,0}}{m_2 - m_1}\right)(m_1 + 3)(1 + z)^{-m_1} + \left(\frac{(m_1 + 3 + 3w_x)\rho_{x,0} + (m_1 + 3)\rho_{c,0}}{m_1 - m_2}\right)(m_2 + 3)(1 + z)^{-m_2}\right], \tag{16}$$

$$\rho_c = \left(\frac{1}{3w_x}\right)\left[\left(\frac{(m_2 + 3 + 3w_x)\rho_{x,0} + (m_2 + 3)\rho_{c,0}}{m_2 - m_1}\right)(m_1 + 3 + 3w_x)(1 + z)^{-m_1} + \left(\frac{(m_1 + 3 + 3w_x)\rho_{x,0} + (m_1 + 3)\rho_{c,0}}{m_1 - m_2}\right)(m_2 + 3 + 3w_x)(1 + z)^{-m_2}\right]. \tag{17}$$

Furthermore, in terms of the new quantities (ρ_1, ρ_2, m_1, m_2), the usual density parameters for dark energy and dark matter at the current time are calculated as

$$\Omega_{x,0} = -\left(\frac{1}{3w_x}\right)[\Omega_1(m_1+3)+\Omega_2(m_2+3)], \tag{18}$$

$$\Omega_{c,0} = \left(\frac{1}{3w_x}\right)[\Omega_1(m_1+3+3w_x)+\Omega_2(m_2+3+3w_x)], \tag{19}$$

with $\Omega_{x,0}+\Omega_{c,0}=\Omega_1+\Omega_2$, where $(\Omega_1,\Omega_2)=(\rho_1/\rho_0, \rho_2/\rho_0)$ and $\rho_0=3H_0^2/8\pi G$. We note that by solving the above equations (18) and (19) one can easily find $\Omega_1=\Omega_1(m_1,m_2,w_x)$ and $\Omega_2=\Omega_2(m_1,m_2,w_x)$. The explicit forms for Ω_1 and Ω_2 are $\Omega_1=\frac{(m_2+3+3w_x)\Omega_{x,0}+(m_2+3)\Omega_{c,0}}{m_2-m_1}$ and $\Omega_2=\frac{(m_1+3+3w_x)\Omega_{x,0}+(m_1+3)\Omega_{c,0}}{m_1-m_2}$. In particular, we consider the case when dark energy is the cosmological constant, i.e., the case when $w_x=-1$. For convenience, we label the interacting dark energy scenario where DE is not the cosmological constant (i.e., $w_x\neq-1$) as IDE, and we label the interacting vacuum scenario where DE is represented by the cosmological constant itself as IVS.

IV. DYNAMICS AT LARGE SCALES: COSMOLOGICAL PERTURBATIONS

The study of cosmological perturbations unveils the hidden nature of the model. Thus, large-scale stability has been a very important way to check the viability of any cosmological model; indeed, for coupled dark energy one needs to check this as well. In particular, we are interested in structure formation when the background has a coupling between dark matter and dark energy governed by the interaction rate specified in Eq. (8). Thus, we consider the perturbed FLRW metric with scalar mode k as [72–74]

$$ds^2 = a^2(\tau)[-(1+2\phi)d\tau^2+2\partial_i B d\tau dx^i + ((1-2\psi)\delta_{ij}+2\partial_i\partial_j E)dx^i dx^j], \tag{20}$$

where ϕ, B, ψ, and E, are the gauge-dependent scalar perturbation quantities and τ is the conformal time. Thus, by using the metric (20) one can find the perturbed equations [33,69,75],

$$\nabla_\nu T_A^{\mu\nu} = Q_A^\mu, \qquad \sum_A Q_A^\mu = 0,$$

where A represents the fluid (dark matter or dark energy) and $Q_A^\mu=(Q_A+\delta Q_A)u^\mu+F_A^\mu$, where Q_A is the energy transfer rate and $F_A^\mu=a^{-1}(0,\partial^i f_A)$ is the momentum density transfer relative to the four-velocity u^μ. (For more discussions in this direction, we refer to the earlier works [33,69,75].) We consider that in the rest frame of dark matter, the momentum transfer potential is zero [33,69,76]. Thus, the momentum transfer potential becomes $k^2 f_A = Q_A(\theta-\theta_c)$. The pressure perturbation is defined by [69,77,78]

$$\delta p_A = c_{sA}^2\delta\rho_A + (c_{sA}^2-c_{aA}^2)\rho_A'(v_A+B), \tag{21}$$

where c_{aA}^2 is the square of the physical sound speed of the fluid "A" in the rest frame and it is defined as $c_{aA}^2=p_A'/\rho_A'=w_x+w_x'/(\rho_A'/\rho_A)$. Now, introducing the density perturbation by $\delta_A=\delta\rho_A/\rho_A$ and considering no contribution from the anisotropic stress, i.e., $\pi_A=0$, the density perturbation and the velocity perturbation equations for the dark matter and dark energy fluids are [33,69,75]

$$\delta_A' + 3\mathcal{H}(c_{sA}^2-w_A)\delta_A + 9\mathcal{H}^2(1+w_A)(c_{sA}^2-c_{aA}^2)\frac{\theta_A}{k^2} + (1+w_A)\theta_A - 3(1+w_A)\psi' + (1+w_A)k^2(B-E') = \frac{a}{\rho_A}(\delta Q_A - Q_A\delta_A) + \frac{aQ_A}{\rho_A}\left[\phi+3\mathcal{H}(c_{sA}^2-c_{aA}^2)\frac{\theta_A}{k^2}\right], \tag{22}$$

$$\theta_A' + \mathcal{H}(1-3c_{sA}^2)\theta_A - \frac{c_{sA}^2}{1+w_A}k^2\delta_A - k^2\phi = \frac{a}{(1+w_A)\rho_A}[(Q_A\theta-k^2 f_A)-(1+c_{sA}^2)Q_A\theta_A], \tag{23}$$

where the new quantities c_{sA}^2 and c_{aA}^2, are the adiabatic and physical sound velocity for the fluid A, respectively, and $\theta=\theta_\mu^\mu$ is the volume expansion scalar. Let us note that to avoid any kind of instabilities, $c_{sA}^2\geq 0$ has been imposed. We also note that here $c_{sc}^2=0$ since we assume cold dark matter (i.e., $w_c=0$). In the synchronous gauge, (i.e., $\phi=B=0$, $\psi=\eta$, and $k^2E=-h/2-3\eta$), the density and the velocity perturbations for the dark fluids are

$$\delta_x' = -(1+w_x)\left(\theta_x+\frac{h'}{2}\right) - 3\mathcal{H}(c_{s,x}^2-w_x)\left[\delta_x+3\mathcal{H}(1+w_x)\frac{\theta_x}{k^2}\right] - 3\mathcal{H}w_x'\frac{\theta_x}{k^2} + \frac{aQ}{\rho_x}\left[-\delta_x+\frac{\delta Q}{Q}+3\mathcal{H}(c_{s,x}^2-w_x)\frac{\theta_x}{k^2}\right], \tag{24}$$

$$\theta_x' = -\mathcal{H}(1-3c_{s,x}^2)\theta_x + \frac{c_{s,x}^2}{(1+w_x)}k^2\delta_x + \frac{aQ}{\rho_x}\left[\frac{\theta_c-(1+c_{s,x}^2)\theta_x}{1+w_x}\right], \tag{25}$$

$$\delta_c' = -\left(\theta_c+\frac{h'}{2}\right)+\frac{aQ}{\rho_c}\left(\delta_c-\frac{\delta Q}{Q}\right), \tag{26}$$

$$\theta_c' = -\mathcal{H}\theta_c, \tag{27}$$

where the term $\delta Q/Q$ includes the perturbation term for the Hubble expansion rate δH. Now by inserting the interaction

rate (8) into the above equations, one can write down the explicit perturbation equations as

$$\delta_x' = -(1+w_x)\left(\theta_x + \frac{h'}{2}\right) - 3\mathcal{H}(c_{sx}^2 - w_x)\left[\delta_x + 3\mathcal{H}(1+w_x)\frac{\theta_x}{k^2}\right] + 3\mathcal{H}\xi\left[\frac{\rho_c}{\rho_x} + (1+w_x)\right]\left[\frac{\rho_c(\delta_c - \delta_x)}{\rho_c + (1+w_x)\rho_x} + \frac{\theta + h'/2}{3\mathcal{H}} + 3\mathcal{H}(c_{sx}^2 - w_x)\frac{\theta_x}{k^2}\right], \quad (28)$$

$$\theta_x' = -\mathcal{H}(1 - 3c_{sx}^2)\theta_x + \frac{c_{sx}^2}{(1+w_x)}k^2\delta_x + 3\mathcal{H}\xi\left[\frac{\rho_c}{\rho_x(1+w_x)} + 1\right][\theta_c - (1+c_{sx}^2)\theta_x], \quad (29)$$

$$\delta_c' = -\left(\theta_c + \frac{h'}{2}\right) + 3\mathcal{H}\xi\left[1 + (1+w_x)\frac{\rho_x}{\rho_c}\right] \times \left[\frac{(1+w_x)\rho_x(\delta_c - \delta_x)}{\rho_c + (1+w_x)\rho_x} - \frac{\theta + h'/2}{3\mathcal{H}}\right], \quad (30)$$

$$\theta_c' = -\mathcal{H}\theta_c. \quad (31)$$

Let us now focus on the growth rate of matter perturbations for the prescribed interaction in this work. Here, we neglect the clustering of dark energy with the assumption that $c_{sx}^2 = 1$. However, depending on the strength of the interaction, the dark energy perturbations could be an important issue, but on the sub-Hubble scale such perturbations are not important provided that the sound speed of the dark energy perturbations is assumed to be positive [76]. The evolution equation for δ_c can be written as

$$\delta_c'' + \left\{1 - 3\xi\left[1 + (1+w_x)\frac{\rho_x}{\rho_c}\right]\right\}\mathcal{H}\delta_c' = 4\pi G a^2\rho_b\delta_b + 4\pi G a^2\rho_c\delta_c\left\{1 + 2\xi\frac{\rho_t}{\rho_c}\left[1 + (1+w_x)\frac{\rho_x}{\rho_c}\right] \times \left[\frac{\mathcal{H}'}{\mathcal{H}^2} + 1 - 3w_x + 3\xi\left(1 + \frac{\rho_x}{\rho_c}\right) + 3\xi(1+w_x)\frac{\rho_x}{\rho_c}\left(1 + \frac{\rho_x}{\rho_c}\right)\right]\right\}, \quad (32)$$

where $\mathcal{H} = aH$ is the conformal Hubble parameter and H can be found from Eq. (4). It is evident that by putting $\xi = 0$ into Eq. (32), one gets back the evolution equation for δ_c for the noninteracting cosmologies, i.e., $\delta_m'' + \mathcal{H}\delta_m' = 4\pi G\rho_m\delta_m$ (note that $\rho_m = \rho_c + \rho_b$). Furthermore, one can also measure the deviations in the expansion history through

$$\frac{\mathcal{H}_{\rm eff}}{\mathcal{H}} = 1 - 3\xi\left[1 + (1+w_x)\frac{\rho_x}{\rho_c}\right], \quad (33)$$

and also in the gravitational constant G as

$$\frac{G_{\rm eff}}{G} = 1 + 2\xi\left(\frac{\rho_t}{\rho_c}\right)\left[1 + (1+w_x)\frac{\rho_x}{\rho_c}\right]\left[\frac{\mathcal{H}'}{\mathcal{H}^2} + 1 - 3w_x + 3\xi\left(1 + \frac{\rho_x}{\rho_c}\right) + 3\xi(1+w_x)\frac{\rho_x}{\rho_c}\left(1 + \frac{\rho_x}{\rho_c}\right)\right]. \quad (34)$$

One can see that $\xi = 0$ in both Eqs. (33) and (34) recovers the standard evolutions of the corresponding quantities where no interaction is present. Further, we consider the growth rate of cold dark matter defined by $f_c \equiv \frac{d}{d\ln a}(\ln\delta_c)$. One may notice that the presence of an interaction in the dark sector automatically modifies the Euler equation, which means that the dark matter may not follow the geodesics [76]. Thus, in the presence of interaction, the above quantities give a qualitative picture of the interaction rate and its behavior compared to the noninteracting cosmologies quantified by $\xi = 0$.

Let us first focus on the dynamics of the IDE model on large scales. The behavior of this model is shown through the evolution of the CMB TT spectra and the matter power spectra. In the left panel of Fig. 1, we show the behavior of the IDE model through the CMB TT spectra which shows that as long as the coupling strength of the interaction increases, the model significantly deviates from the noninteracting ΛCDM model. The deviation is also clear from the relative deviation $\Delta C_l^{\rm TT}/C_l^{\rm TT}$ (here $\Delta C_l^{\rm TT}$ measures the deviation of the model from ΛCDM), and one can see that a nonzero deviation from ΛCDM is prominent for all of the coupling parameters considered in the analysis, which is evident from the low multipoles l. On the other hand, for large coupling strength, the model significantly deviates from ΛCDM, which is clear from both the left and right panels of Fig. 1. Similarly, for different coupling strengths of the interaction rate, we show the evolution of the matter power spectra in the left panel of Fig. 2. Again we see that for a large coupling strength, the model significantly deviates from ΛCDM cosmology and this deviation is prominent for large k, while for very small coupling the interaction model is very close to ΛCDM. However, the deviation from ΛCDM—even for a very small but nonzero coupling strength—still exists, which is clear from the relative deviation shown in the right panel of Fig. 2. From the

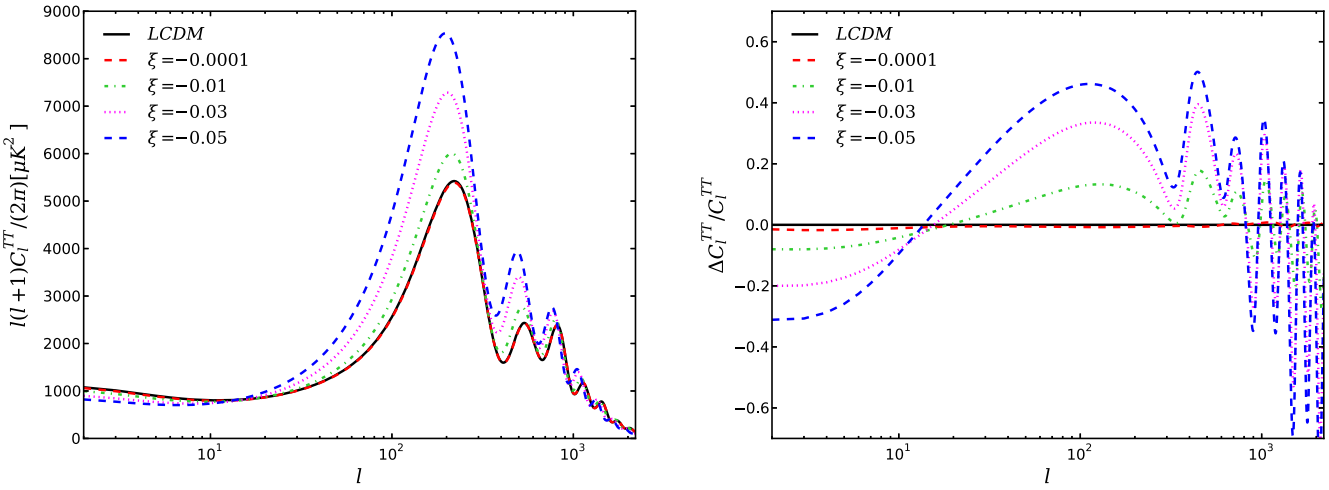

FIG. 1. The behavior of the IDE scenario on large scales is shown for different values of the coupling parameter ξ. Left panel: Here we display the evolutions of the CMB TT spectra for different values of the coupling parameter representing its strength. We see that as the magnitude of the coupling parameter increases, the interaction scenario effectively deviates from the usual noninteracting ΛCDM cosmology. We note that the curves representing $\xi = -0.0001$ and ΛCDM are almost indistinguishable from one another. Right panel: Here, the relative deviation in the CMB TT spectra is compared to the noninteracting ΛCDM model. This confirms the observation found in the left panel of this figure. In this figure, we observe that a very small difference between the curves representing $\xi = -0.0001$ and ΛCDM exists, but it is very hard to detect.

analyses using both CMB and matter power spectra as well as the corresponding relative deviations, one may argue that the coupling strength $\xi = -0.05$ is very high and can be excluded from the picture.

Furthermore, we depict the modified expansion history $\mathcal{H}_{\rm eff}$ [Eq. (33)] and the effective gravitational constant [Eq. (34)] in the left and right panels of Fig. 3, respectively. Both plots in Fig. 3 show that for large coupling strength, the modified expansion history and the effective gravitational constant significantly differ from that of the noninteracting ΛCDM cosmology. Finally, from the growth rate of cold dark matter, f_c, displayed in Fig. 4 we observe a similar trend: a large coupling strength implies a deviation of the model from noninteracting ΛCDM cosmology. We conclude that for large coupling strength, the growth rate of cold dark matter significantly decreases.

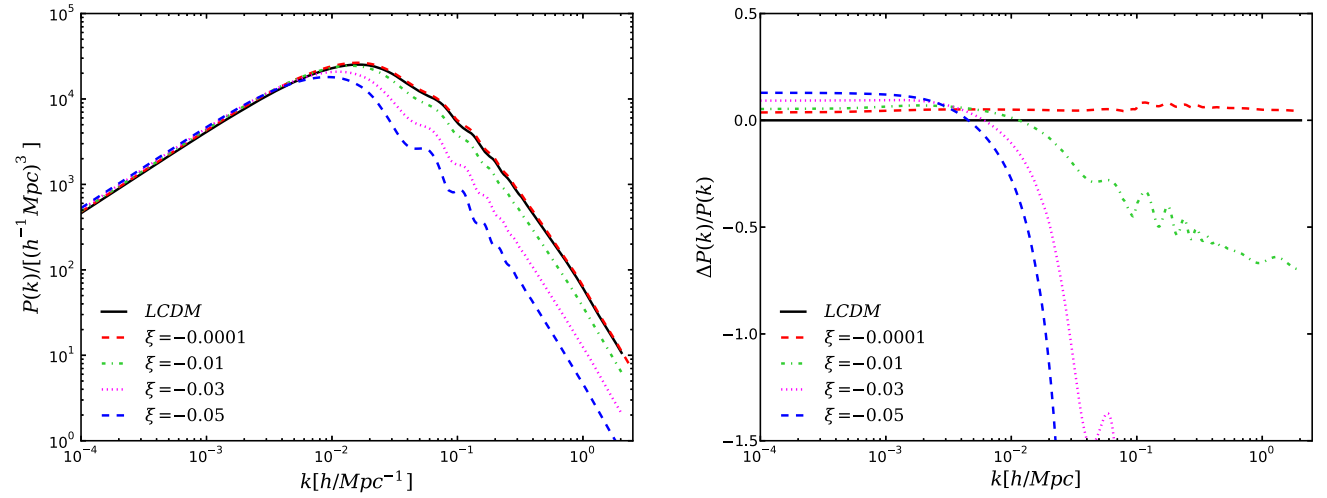

FIG. 2. The behavior of the IDE scenario on large scales is shown for different values of the coupling parameter. Left panel: We show the evolutions of the matter power spectra for different coupling strengths of the interaction model. We find that as the coupling strength increases, the interaction scenario deviates from the usual noninteracting ΛCDM scenario (i.e., $\xi = 0$). We note that the curves representing $\xi = -0.0001$ and ΛCDM are almost indistinguishable from one another. Right panel: The relative deviation in the matter power spectra compared to the noninteracting ΛCDM model is shown, and we find similar observation as in the left panel. In this figure, we observe that a very small difference between the curves representing $\xi = -0.0001$ and ΛCDM exists, and it is clearly visible.

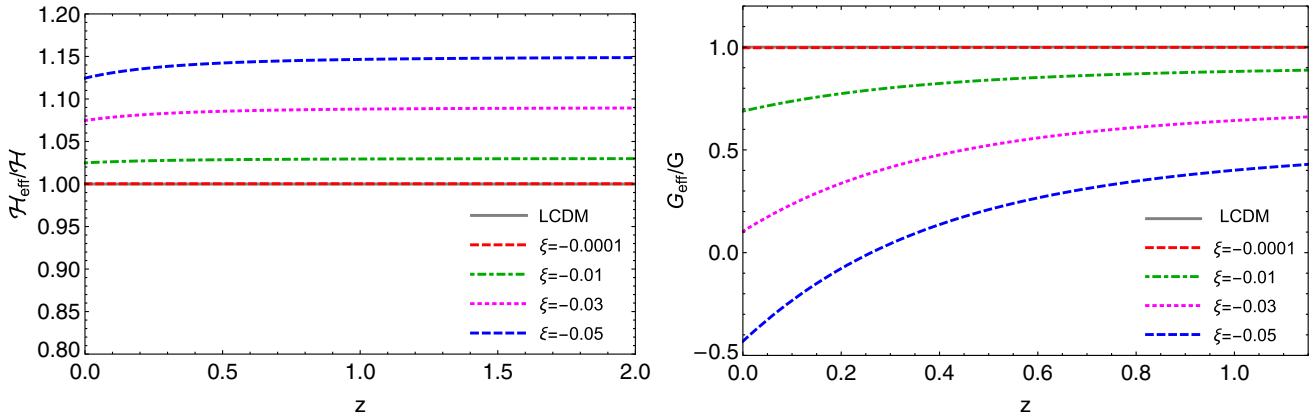

FIG. 3. Left panel: The dynamical evolution of the quantity $\mathcal{H}_{\rm eff}/\mathcal{H}$ is shown for different values of the coupling parameter of the interaction rate (8). From top to bottom, the curves stand for the ΛCDM ($\xi = 0$) model, $\xi = -0.0001$, -0.01, -0.03, and -0.05. We notice that the curves representing noninteracting ΛCDM and $\xi = -0.0001$ are practically indistinguishable from one another. Right panel: The evolution of the quantity $G_{\rm eff}/G$ is shown for different values of the coupling parameter of the interaction rate (8). From top to bottom, the curves stand for the ΛCDM ($\xi = 0$) model, $\xi = -0.0001$, -0.01, -0.03, and -0.05. Similar to the left panel, here we also notice that the curves representing ΛCDM and $\xi = -0.0001$ are practically indistinguishable from each other. From both panels, we see that as ξ increases the model deviates from the noninteracting ΛCDM cosmology, and the coupling parameter $\xi = -0.05$ can be safely excluded from the consideration.

The dynamics of this interaction scenario on large scales has also been investigated. In the left panel of Fig. 5 we show the variation in the CMB TT spectra for different strengths of the coupling parameter ξ and compare them with the noninteracting ΛCDM scenario. We see that as ξ increases a significant change in the CMB TT spectra is observed with respect to the noninteracting scenario, while for lower coupling strengths the deviation from the noninteracting ΛCDM model is small. However, since the observational data predict a very small coupling parameter (allowing for a zero value at the 68.3% confidence level), it is expected that a small deviation from the ΛCDM model should be present. In order to measure such a small deviation, we measure the relative deviation of the interacting model with different coupling strengths with respect to the ΛCDM model; this is shown in the right panel of Fig. 5. This plot practically tells that for $\xi \neq 0$; however small it is, a deviation from ΛCDM should exist, although it is also true that such a deviation would be very small and thus is not very significant. A similar pattern is found when the large-scale dynamics is described in terms of the matter power spectra shown in Fig. 6. The left panel of Fig. 6 shows qualitative changes in the matter power spectra for different coupling strengths, while the right panel shows how much the model with different coupling strengths differs from ΛCDM. Overall, from the analyses for IVS one can see that the coupling strength $\xi = -0.05$ presents a significant deviation from ΛCDM cosmology which—according to the present observational data—is not reliable; hence, this large value of the coupling parameter should be avoided. Finally, following the similar lines as in IDE, for IVS we investigate the modified expansion history (left panel of Fig. 7), the effective gravitational constant (right panel of Fig. 7) as well as the growth rate of cold dark matter, f_c (Fig. 8) finding that for large coupling strength, the model considerably deviates from the noninteracting ΛCDM model.

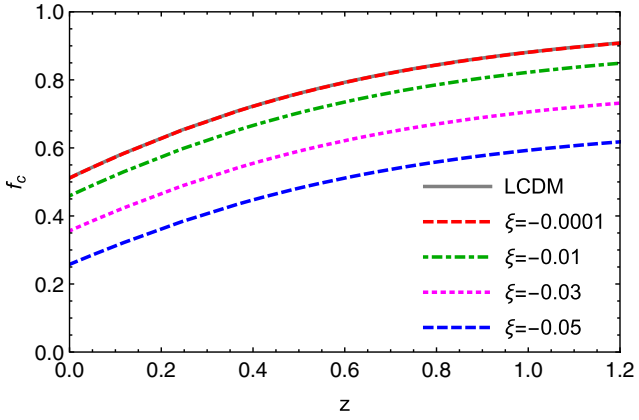

FIG. 4. The evolution of growth rate for cold dark matter in the presence of the interaction rate (8) is shown for different values of the coupling strength. From top to bottom, the curves stand for the noninteracting ΛCDM model (where $\xi = 0$) and with other coupling parameters $\xi = -0.0001$, -0.01, -0.03, and -0.05. Here, too, the curves for ΛCDM and $\xi = -0.0001$ are indistinguishable from each other. From the figure we observe that as long as the strength or magnitude of the coupling parameter increases, the growth rate for the cold dark matter sector significantly deviates from $\xi = 0$ (no interaction, ΛCDM). The physical scenario indicates that as the coupling strength increases, the growth rate for the cold dark matter decreases with the evolution of the universe.

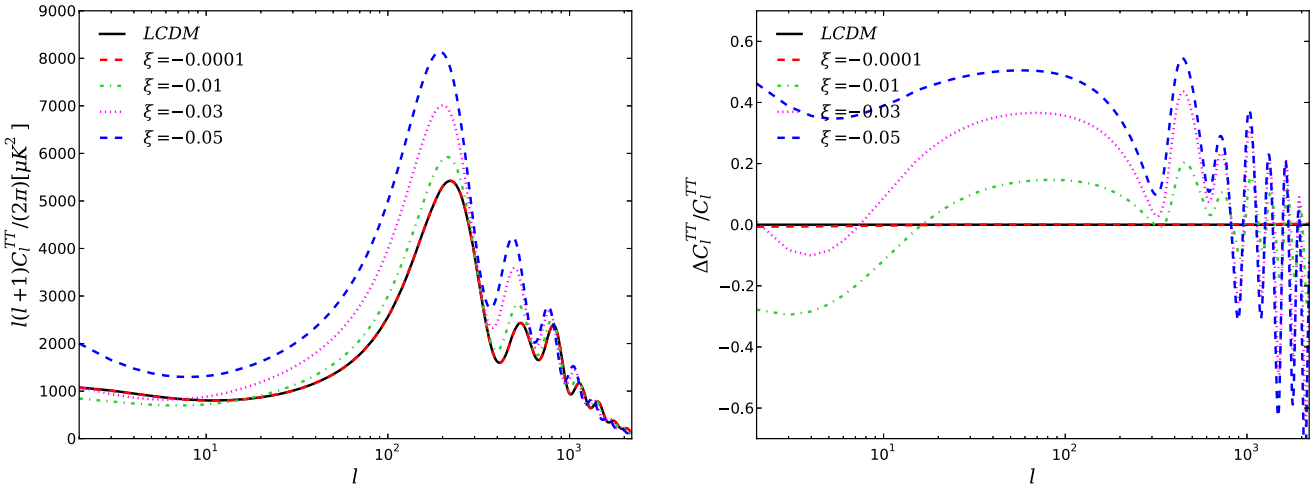

FIG. 5. The behavior of the IVS on large scales is shown for different values of the coupling parameter ξ. Left panel: In this plot, we show the evolutions of the CMB TT spectra for different coupling strengths of the interaction model. One can clearly see that as the magnitude or strength of the coupling parameter increases, the interaction model clearly deviates from the noninteracting ΛCDM cosmology. We note that the curves representing $\xi = -0.0001$ and ΛCDM cannot be differentiated from one another. Right panel: The relative deviation in the CMB TT spectra is compared to the noninteracting ΛCDM model. From this plot, one can easily conclude that changes in ξ result in significant deviations from the corresponding noninteracting scenario. Here, we observe that the curves representing $\xi = -0.0001$ and ΛCDM overlap with each other.

V. DATA AND RESULTS

In this section, we describe the astronomical data using statistical techniques to constrain the present interacting scenarios and the results of the analyses. We include the following sets of astronomical data.

(1) *CMB observations:* We use CMB data from Planck's 2015 observations [79,80]. In particular, we use the likelihoods C_l^{TT}, C_l^{EE}, and C_l^{TE} in addition to low-l polarization data (i.e., Planck TT, TE, EE + low TEB).

(2) *Baryon acoustic oscillation (BAO) data:* For BAO data, the estimated ratio r_s/D_V is used as a "standard ruler" in which r_s is the comoving sound horizon at the baryon drag epoch and D_V is the effective distance, given by $D_V(z) = [(1+z)^2 D_A(a)^2 \frac{z}{H(z)}]^{1/3}$. Here D_A is the angular diameter distance. In this analysis we

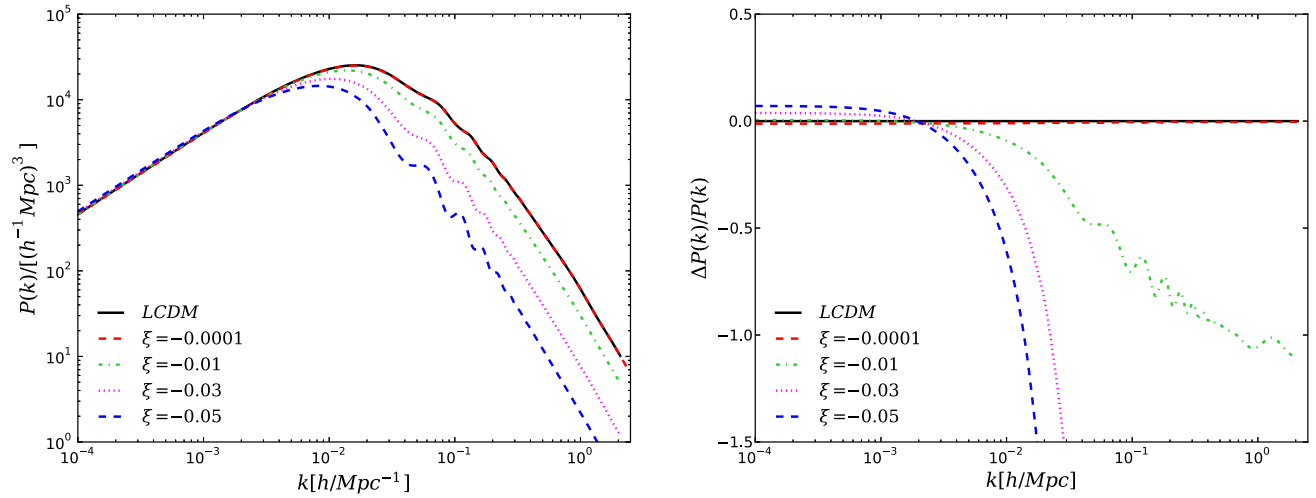

FIG. 6. The behavior of the IVS on large scales is shown for different values of the coupling parameter ξ. Left panel: We show the evolutions of the matter power spectra for different coupling strengths of the interaction model which shows that as the coupling parameter increases, the interaction model deviates from the noninteracting ΛCDM cosmology. We notice that the curves representing $\xi = -0.0001$ and ΛCDM cannot be differentiated from one another. Right panel: The relative deviation in the matter power spectra is compared to the noninteracting ΛCDM model, and similar features are observed as in the left panel of this figure. From this plot we see that the curves representing $\xi = -0.0001$ and ΛCDM cannot be distinguished from one another, although a very minimal difference between them is present.

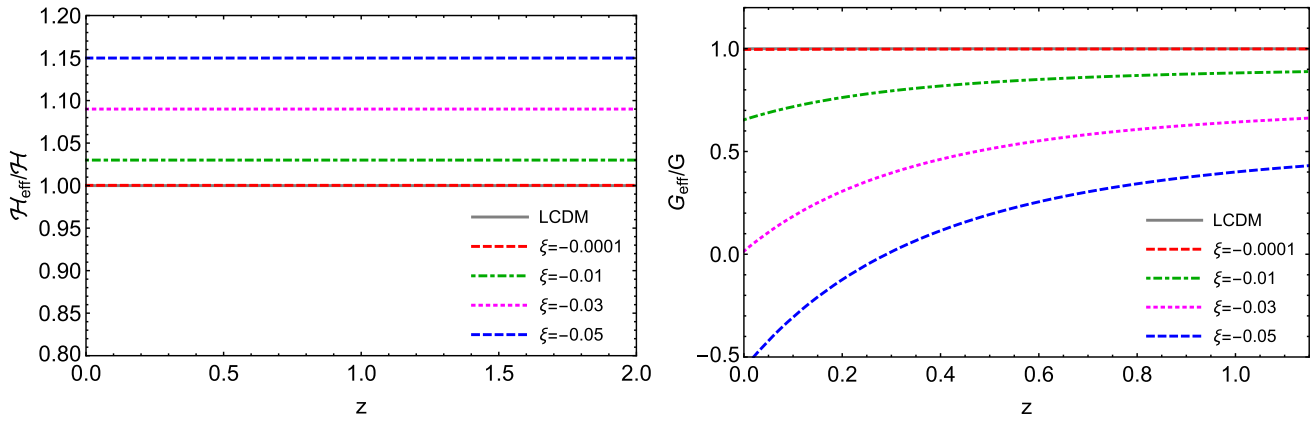

FIG. 7. Left panel: The dynamical evolution of the modified expansion history $\mathcal{H}_{\rm eff}$ is shown in the presence of different couplings of the interaction rate (8) for the interacting vacuum scenario. From top to bottom, the curves stand for the noninteracting ΛCDM model ($\xi = 0$) and for $\xi = -0.0001$, -0.01, -0.03, and -0.05. Right panel: The evolution of the quantity $G_{\rm eff}/G$ is shown for different coupling parameters for the interacting vacuum scenario. From top to bottom, the curves stand for the noninteracting ΛCDM model ($\xi = 0$) and for $\xi = -0.0001$, -0.01, -0.03, and -0.05. From both panels, we see that as ξ increases, the model deviates from the noninteracting ΛCDM cosmology. In both panels, we see that the curves representing $\xi = -0.0001$ and ΛCDM cannot be differentiated from one another.

use four data points from different astronomical surveys: the 6dF Galaxy Survey redshift measurement at $z_{\rm eff} = 0.106$ [81], the Main Galaxy Sample of Data Release 7 of the Sloan Digital Sky Survey measurement at $z_{\rm eff} = 0.15$ [82], and the CMASS and LOWZ samples from the latest Data Release 12 (DR12) of the Baryon Oscillation Spectroscopic Survey (BOSS) measurements at $z_{\rm eff} = 0.57$ [83] and $z_{\rm eff} = 0.32$ [83].

(3) *Redshift space distortion (RSD) data:* We use the RSD data from two observational surveys: the CMASS sample [84] and the LOWZ sample [84]. The effective redshifts for the CMASS and LOWZ samples are, respectively, at $z_{\rm eff} = 0.57$ and $z_{\rm eff} = 0.32$. We note that when these two RSD data points are considered in the analysis, DR12 of BOSS from BAO will not be considered.

(4) *H_0 from the Hubble Space Telescope (HST):* The local Hubble constant measured using the HST by Riess *et al.* [85] yields $H_0 = 73.02 \pm 1.79$ km/s/Mpc with 2.4% precision.

(5) *Joint light curve analysis (JLA):* This is the type Ia supernovae sample that contains 740 data points spread over the redshift interval $z \in [0.01, 1.30]$ [86]. This low-redshift sample is the first indication of an accelerating Universe.

(6) *Hubble parameter measurements from cosmic chronometers (CC):* We choose the cosmic chronometers to measure the Hubble parameter values at different redshifts. Cosmic chronometers are the oldest and most massive galaxies, and the technique that we apply to measure the Hubble parameter values is the differential age evolution of the galaxies. For a detailed description, we refer to Ref. [87] and references therein for more information about their implementation. In this work we consider 30 Hubble parameter values in the interval $z \in (0, 2)$ and they can be found in Ref. [87].

(7) *Weak lensing (WL):* We use the weak gravitational lensing data from the Canada-France-Hawaii Telescope Lensing Survey [88,89].

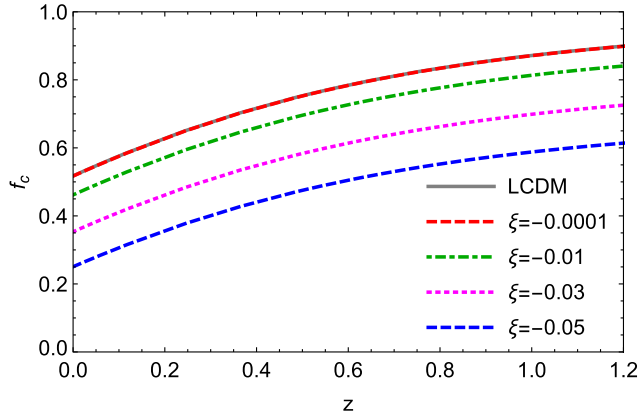

FIG. 8. For the interacting vacuum scenario we display the evolution of the growth rate for cold dark matter for different coupling strengths. From top to bottom, the curves stand for the noninteracting ΛCDM model ($\xi = 0$) and for $\xi = -0.0001$, -0.01, -0.03, and -0.05. However, we observe that if the coupling strength increases, the growth rate for cold dark matter decreases with the evolution of the universe. Similar to previous observations, here we see that the curves representing $\xi = -0.0001$ and ΛCDM cannot be distinguished from one another.

In order to extract the observational constraints of the interacting scenarios, we use the publicly available Monte Carlo Markov chain (MCMC) package CosmoMC [90,91] equipped with a convergence diagnostic followed by the Gelman-Rubin statistics [92]. The parameter space for the interacting dark energy and interacting vacuum scenarios are, respectively,

TABLE I. This table summarizes the flat priors on the cosmological parameters for the interacting scenario with $w_x < -1$ (IDE) and the IVS.

Parameter	Prior (IDE)	Prior (IVS)
$\Omega_b h^2$	[0.005, 0.1]	[0.005, 0.1]
τ	[0.01, 0.8]	[0.01, 0.8]
n_s	[0.5, 1.5]	[0.5, 1.5]
$\log[10^{10}A_s]$	[2.4, 4]	[2.4, 4]
$100\theta_{MC}$	[0.5, 10]	[0.5, 10]
w_x	$(-3,-1)$	–
ξ	$[-1,0]$	$[-1,0]$

$$\mathcal{P}_1 \equiv \{\Omega_b h^2, \Omega_c h^2, 100\theta_{MC}, \tau, w_x, \xi, n_s, \log[10^{10}A_S]\} \quad (35)$$

and

$$\mathcal{P}_2 \equiv \{\Omega_b h^2, \Omega_c h^2, 100\theta_{MC}, \tau, \xi, n_s, \log[10^{10}A_S]\}, \quad (36)$$

where in both Eqs. (35) and (36), $\Omega_b h^2$ and $\Omega_c h^2$ are the baryon density and cold dark matter density, respectively; $100\theta_{MC}$, τ, n_s, and A_S, are the ratio of the sound horizon to the angular diameter distance, optical depth, scalar spectral index, and the amplitude of the initial power spectrum, respectively. The parameter ξ is the coupling strength, while $\mathcal{P}_1$ has one extra parameter w_x. Thus, we see that interacting dark energy has eight free parameters and the interacting vacuum scenario has seven free parameters. During the MCMC analysis, we generally fix some priors on the model parameters. In Table I we show the priors fixed on various cosmological parameters while constraining both interacting models (IDE and IVS). The priors on w_x and ξ play an essential role in the analysis because the early-time instabilities associated with the model, if any, significantly depend on the parameter space of (w_x, ξ). Now, if we look closely at the model (9), we can see that it actually incorporates two separate interaction rates, namely, $Q \propto \rho_c$ and $Q \propto \rho_x$; hence, the stability of the entire model (9) depends on the region where both of them do not lead to any early-time instabilities. However, one can note that for some specific regions of the parameter space of w_x and ξ early-time instabilities can be avoided [93], while the entire region for ξ that allows both positive and negative values may not always be suitable for avoiding such an instability. This actually depends on the interaction model. Thus, motivated by this fact, we divide the parameter space of w_x and ξ into several regions to test the stability of the IDE scenario: "w_x free and ξ free," "$w_x > -1$ and ξ free," "$w_x > -1$ and $\xi \geq 0$," "$w_x > -1$, $\xi \leq 0$," "$w_x < -1$ and ξ free," and "$w_x < -1$ and $\xi \leq 0$." We find that the model does not lead to any early-time instabilities only for the region "$w_x < -1$, $\xi \leq 0$," while for the other regions the model leads to early-time instabilities. Quite interestingly, this allowed region (i.e., $w_x < -1$) has an additional feature: in the presence of a nongravitational interaction in the dark sectors, when the dark energy equation of state is allowed to cross the cosmological constant boundary (that is, for $w_x < -1$), the tension on H_0 can be alleviated [20,94]. In this context we would like to add that some previous studies found that for noninteracting cosmologies with a constant dark energy equation of state (w_x) the region $w_x > -1$ is also allowed and even preferred by some observational data [95–97]. Now, we perform similar analyses for the interacting vacuum scenario with different priors on ξ, namely, $\xi \geq 0$, $\xi \leq 0$ and ξ free. We find that for $\xi \leq 0$, early-time instabilities do not appear.

TABLE II. The table summarizes the observational constraints on the cosmological parameters of IDE at the 68.3% confidence level for different combinations of observational data. For the coupling parameter, we only report their values at the 95.4% lower confidence level.

Parameters	CMB	CMB + BAO +HST	CMB + BAO +RSD	CMB + BAO +RSD + HST	CMB + BAO +RSD + HST +JLA + CC	CMB + BAO +RSD + HST +JLA + CC + WL
$\Omega_c h^2$	$0.1260^{+0.0035}_{-0.0059}$	$0.1204^{+0.0017}_{-0.0015}$	$0.1205^{+0.0014}_{-0.0013}$	$0.1201^{+0.0013}_{-0.0014}$	$0.1197^{+0.0012}_{-0.0013}$	$0.1191^{+0.0011}_{-0.0011}$
$\Omega_b h^2$	$0.0223^{+0.0002}_{-0.0002}$	$0.02231^{+0.0002}_{-0.0002}$	$0.0223^{+0.0002}_{-0.0002}$	$0.0223^{+0.0002}_{-0.0002}$	$0.0223^{+0.0002}_{-0.0002}$	$0.0223^{+0.0001}_{-0.0001}$
$100\theta_{MC}$	$1.0310^{+0.0007}_{-0.0005}$	$1.0405^{+0.0006}_{-0.0005}$	$1.0405^{+0.0003}_{-0.0003}$	$1.0405^{+0.0003}_{-0.0003}$	$1.0406^{+0.0003}_{-0.0004}$	$1.0406^{+0.0003}_{-0.0003}$
τ	$0.0711^{+0.0184}_{-0.0187}$	$0.0811^{+0.0214}_{-0.0204}$	$0.0687^{+0.0167}_{-0.0163}$	$0.0621^{+0.0171}_{-0.0160}$	$0.0820^{+0.0164}_{-0.0160}$	$0.0636^{+0.0163}_{-0.0159}$
n_s	$0.9678^{+0.0057}_{-0.0056}$	$0.9739^{+0.0051}_{-0.0051}$	$0.9728^{+0.0039}_{-0.0038}$	$0.9730^{+0.0041}_{-0.0041}$	$0.9746^{+0.0037}_{-0.0035}$	$0.9751^{+0.0037}_{-0.0036}$
$\ln(10^{10}A_s)$	$3.0824^{+0.0356}_{-0.0362}$	$3.1032^{+0.0418}_{-0.0386}$	$3.0770^{+0.0349}_{-0.0316}$	$3.0642^{+0.0338}_{-0.0309}$	$3.1043^{+0.0332}_{-0.0314}$	$3.0658^{+0.0318}_{-0.0308}$
Ω_{m0}	$0.3523^{+0.0394}_{-0.0693}$	$0.2865^{+0.0092}_{-0.0092}$	$0.3105^{+0.0100}_{-0.0098}$	$0.2990^{+0.0083}_{-0.0091}$	$0.2942^{+0.0075}_{-0.0074}$	$0.2994^{+0.0073}_{-0.0073}$
σ_8	$0.8221^{+0.0392}_{-0.0350}$	$0.8635^{+0.0192}_{-0.0192}$	$0.8279^{+0.0137}_{-0.0136}$	$0.8311^{+0.0146}_{-0.0143}$	$0.8516^{+0.0162}_{-0.0160}$	$0.8250^{+0.0132}_{-0.0147}$
H_0	$65.5213^{+4.5145}_{-3.9333}$	$70.7651^{+1.1132}_{-1.1482}$	$67.9685^{+0.8324}_{-1.0243}$	$69.1889^{+0.8698}_{-0.8904}$	$69.6402^{+0.8265}_{-0.8523}$	$68.8940^{+0.6849}_{-0.8176}$
w_x	$-1.1093^{+0.0828}_{-0.0509}$	$-1.1511^{+0.0529}_{-0.0586}$	$-1.0603^{+0.0427}_{-0.0201}$	$-1.0940^{+0.0407}_{-0.0394}$	$-1.0960^{+0.0375}_{-0.0365}$	$-1.0608^{+0.0289}_{-0.0238}$
ξ	> -0.004884	> -0.001285	> -0.001384	> -0.001278	> -0.000959	> -0.000935

A. IDE: Results

In Table II we summarize the 68% confidence-level constraints on the cosmological parameters for $\xi \leq 0$ and $w_x < -1$ using a variety of astronomical data. In Fig. 9 we show the 68.3% and 95.4% confidence-level contour plots for different combinations of the model parameters, including one-dimensional posterior distributions for some selected parameters of the interacting scenario as well. We notice that the combined data set CMB + ext, where "ext" is the combination of any two data sets from BAO, RSD, HST, JLA, CC, WL, significantly reduces the allowed region in the parameter space.

From the analyses presented in Table II, one can easily state that the coupling parameter is very low. The coupling parameter ξ (at the 95.4% lower C.L.) is constrained to be (see Table II)

(1) $\xi > -0.004884$ (CMB only),
(2) $\xi > -0.001285$ (CMB + BAO + HST),
(3) $\xi > -0.001384$ (CMB + BAO + RSD),
(4) $\xi > -0.001278$ (CMB + BAO + RSD + HST),

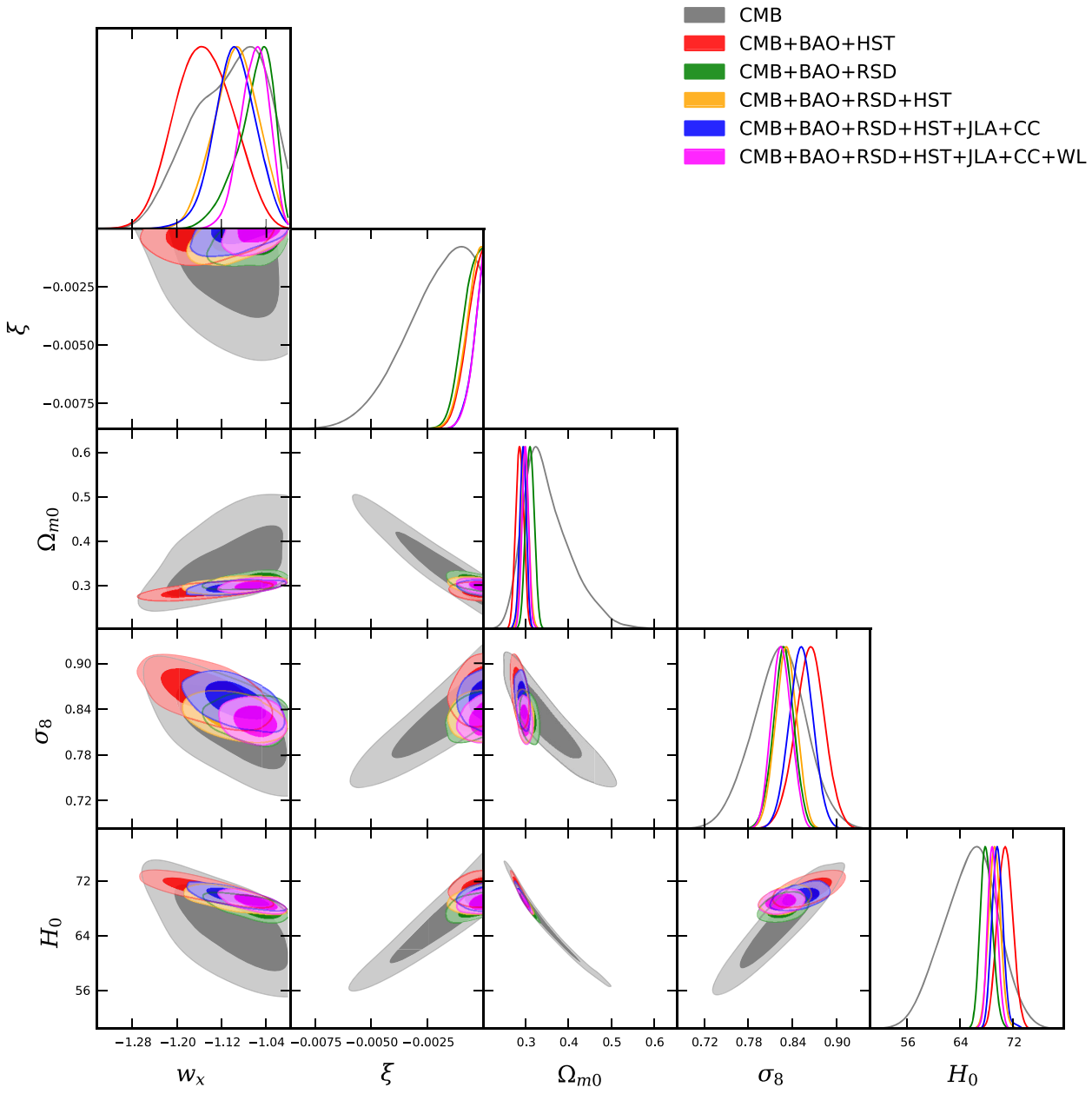

FIG. 9. Contour plots for different combinations of the cosmological parameters at the 68.3% and 95.4% confidence levels are shown for distinct observational combinations. Additionally, we also show the one-dimensional posterior distributions for those parameters in the extreme right corners of each row. From the two-dimensional contour plots one can notice that the addition of any external data to CMB decreases the error bars of the cosmological parameters in a significant way.

(5) $\xi > -0.000959$ (CMB + BAO + RSD + HST + JLA + CC),

(6) $\xi > -0.000935$, for the last combined analysis (CMB + BAO + RSD + HST + JLA + CC + WL),

while we must note that within 68.3% C.L. $\xi = 0$ is allowed, which means that, effectively, IDE may recover the noninteracting w_xCDM cosmology. In Fig. 10, we show the dependence of ξ on the other cosmological parameters for this model. Now, from the constraints on the dark energy equation of state summarized in Table II, it is quite clear that w_x assumes values that are close to -1. To better understand this, in Fig. 11, we show the dependence of w_x on the other important cosmological parameters. From the left panel of Fig. 11 we see that as H_0 decreases, w_x approaches the cosmological constant limit, while from the right panel of Fig. 11 we observe that Ω_{m0} takes large values as $w_x \to -1$. Further, in Fig. 12 we explicitly show the two-dimensional contour plots in the planes (σ_8, w_x), (σ_8, H_0), and (σ_8, ξ) in order to measure the variation in σ_8 in the presence of the coupling. Our analysis shows that an increased coupling strength effectively lowers the values of σ_8, which means that the model deviates significantly from the ΛCDM model. We also observe that for a more phantom state in the dark energy equation of state the value of σ_8 increases. In addition, we also observe that in the presence of the coupling, higher values of the Hubble parameter also indicate higher values of σ_8.

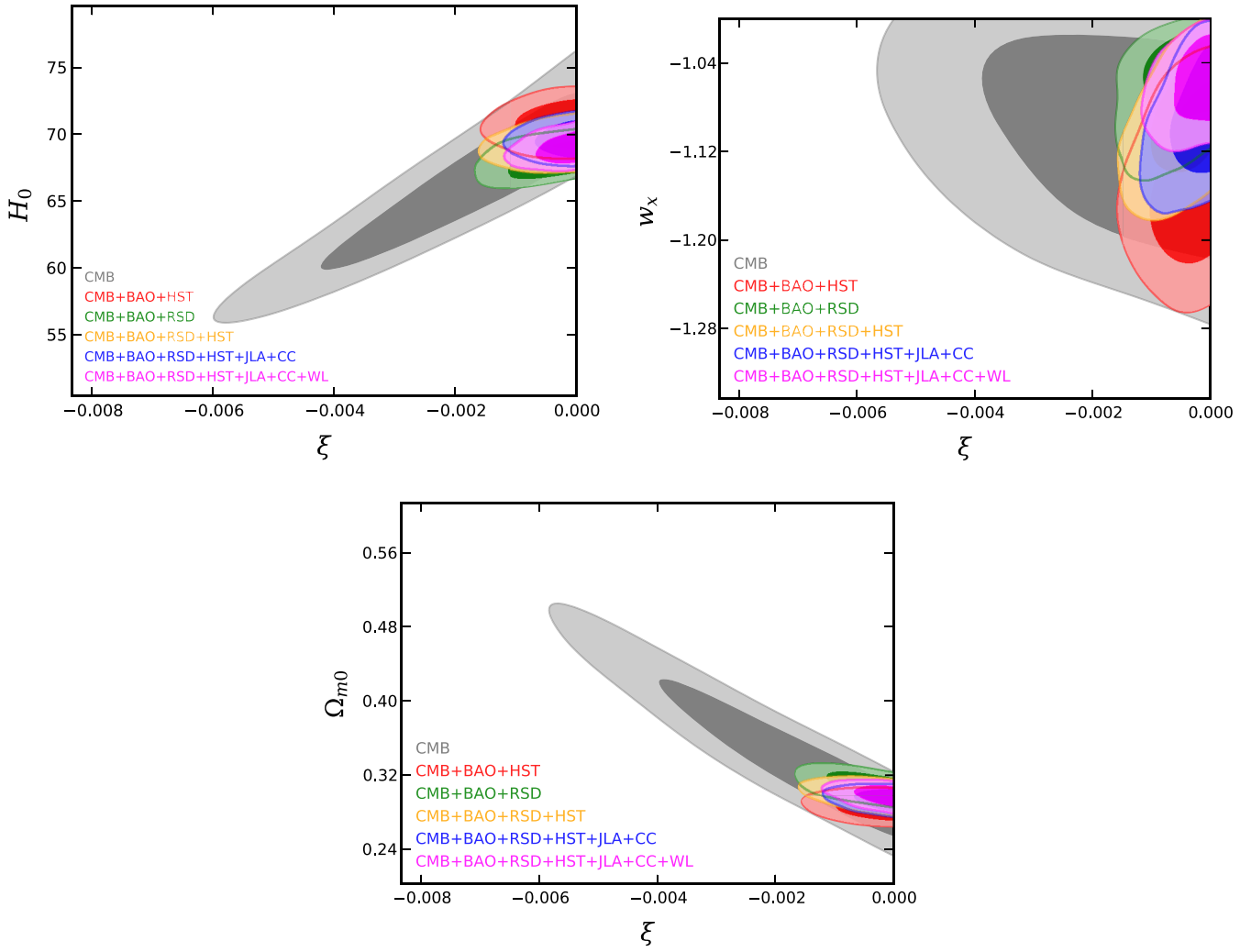

FIG. 10. The dependence of the coupling strength on some important cosmological parameters is shown in the (ξ, H_0), (ξ, w_x), and (ξ, Ω_{m0}) planes at the 68.3% and 95.4% confidence levels using different combinations of the observational data displayed above. We observe that correlations exist between the parameters in the plots. Upper left panel: We see that the CMB data allow a nonzero interaction in the dark sector for lower values of the Hubble parameter; however, from the combined analysis no conclusive statement can be made on the dependence of H_0 and the coupling strength ξ. Upper right panel: The plot shows that the allowance of $w_x < -1$ is an indication of an interaction in the dark sector. Lower panel: One can notice that only CMB data indicate that the coupling strength has a direct dependence on the density parameter Ω_{m0}, while the combined analysis does not show any relation between the parameters. Thus, in order to clarify such issues we show three-dimensional scatter plots in Fig. 13 with detailed discussions.

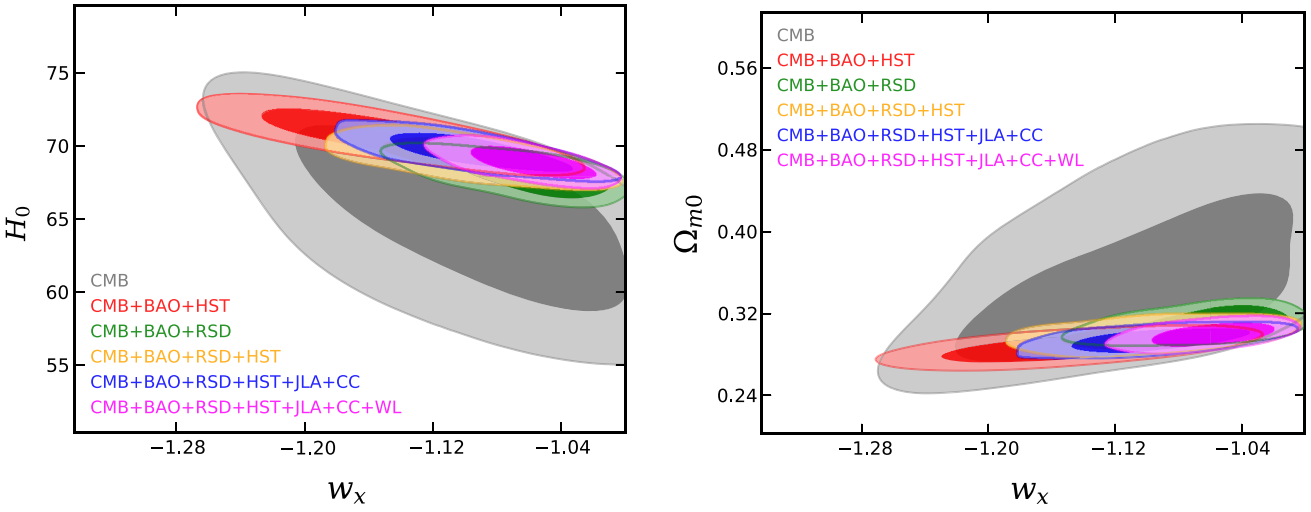

FIG. 11. 68.3% and 95.4% confidence-level contour plots in the two-dimensional planes (w_x, H_0) and (Ω_{m0}, w_x) are shown for different combined analyses. Left panel: Here we notice that for lower values of the Hubble parameter, the dark energy equation of state increases, which means that $|w_x|$ decreases. Right panel: Here we notice that as Ω_{m0} decreases, the dark energy equation of state moves toward a more phantom region.

Furthermore, we analyze the MCMC chains for all combined analyses focusing on the behavior of the coupling strength, dark energy equation of state, and the density parameter for the matter sector monitored by the Hubble parameter values. The analysis is shown in Fig. 13. In particular, this analysis shows the qualitative behavior of the interacting model in terms of the coupling strength and the dark energy equation of state. The analysis shows that the lower values of the Hubble parameter signal a nonzero interaction in the dark sector, but the dark energy equation of state still lies within a close neighborhood of the cosmological constant boundary -1. Also, the density parameter for matter takes larger values for lower values of the Hubble parameter as well.

Last, we compare the $\chi^2_{\rm min}$ values between IDE and the ΛCDM model obtained for different combined analyses (see Table III). We observe that for some combined analyses, the $\chi^2_{\rm min}$ achieved for IDE is bigger than that for the ΛCDM model. We notice that almost all combined analyses return a greater $\chi^2_{\rm min}$ for IDE compared to the standard ΛCDM.

B. IVS: Results

As a particular case, we consider the simplest possibility, i.e., when dark energy is the cosmological constant. Now, we also constrain this interacting scenario using the same combined analyses as employed in Sec. V A. The results are summarized in Table IV, and Fig. 14 shows the two-dimensional contour plots at the 68.3% and 95.4% confidence levels for different combinations of the free model parameters using the six different combined analyses. Additionally, in the extreme right corner of each row of Fig. 14 we show the one-dimensional posterior distributions for some selected model parameters of this interacting scenario. From Fig. 14 we see that the addition of any other external data to CMB significantly decreases the allowed region in the parameter space, and hence the parameters are well constrained when any external data set is added to CMB.

From the analysis we notice that the coupling strength of the interaction is very small and it is very close to zero. In particular, at the 95.4% lower confidence level, we find that

(1) $\xi > -0.001953$ (for CMB alone),
(2) $\xi > -0.000490$ (CMB + BAO + HST),
(3) $\xi > -0.000726$ (CMB + BAO + RSD),
(4) $\xi > -0.000549$ (CMB + BAO + RSD + HST),
(5) $\xi > -0.000563$ (CMB + BAO + RSD + HST+ JLA + CC),
and finally,
(6) $\xi > -0.000557$, for the last combined analysis (CMB + BAO + RSD + HST + JLA + CC + WL).

Additionally, we must mention that within the 68.3% confidence level, the noninteracting scenario (i.e., $\xi = 0$) is recovered (excluding the CMB analysis). Thus, one can see that this interaction scenario is effectively very close to the noninteracting ΛCDM scenario.

Similar to the IDE model described in Sec. V A, here we also investigate the three-dimensional scatter plots in the (ξ, Ω_{m0}) plane for all of the combined analyses colored by the Hubble parameter values. The analysis is shown in Fig. 15 from which one can notice that, for lower values of the Hubble parameter, the coupling parameter seems to have a tendency to take values away from $\xi = 0$, while for higher values of H_0 the coupling parameter takes values very close to zero.

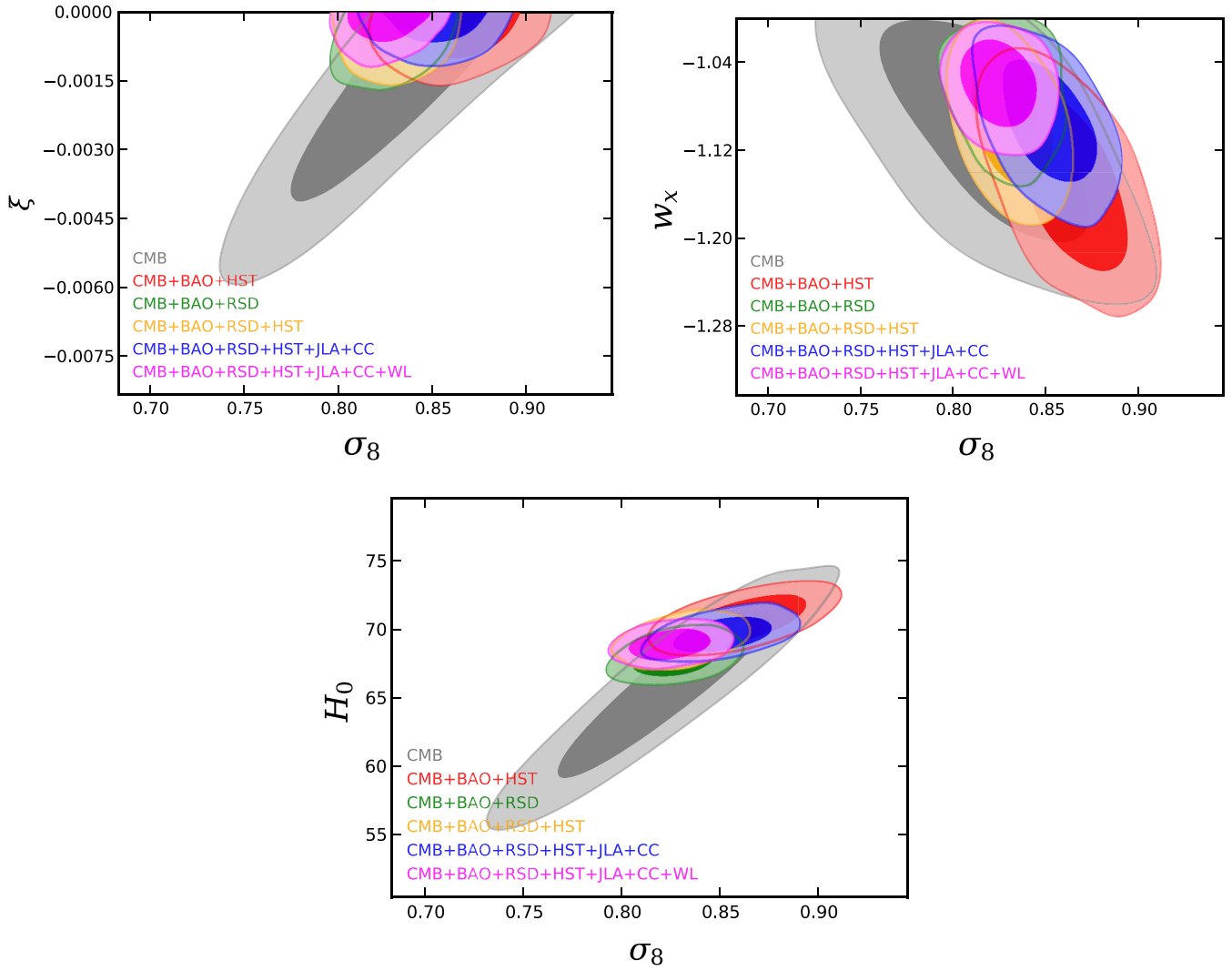

FIG. 12. 68.3% and 95.4% confidence-level contour plots in the two-dimensional planes (σ_8, w_x), (σ_8, H_0), and (σ_8, ξ) are shown. Upper left panel: We notice that if the strength of the interaction increases, σ_8 takes lower values. Upper right panel: It is clearly seen that as long as the dark energy equation of state moves toward a more phantom region, the parameter σ_8 takes larger values. Lower panel: The larger values of the Hubble parameter allow larger values of σ_8.

Similarly to the IDE model, we compare the $\chi^2_{\rm min}$ values for this scenario with respect to the base ΛCDM model. We make similar conclusions for this interaction scenario: the $\chi^2_{\rm min}$ values for this model are larger for almost all combined analyses with respect to the ΛCDM cosmological model.

C. On the tension on H_0: The role of interaction

One of the most popular issues in current cosmological research is the tension on the parameter H_0. Some recent investigations in the context of interacting dark energy models fueled further investigations aiming to reach a definite and satisfactory explanation of this tension, and consequently people have focused on how interacting dark energy models may alleviate the tension on H_0. The first question that immediately arises is what exactly this tension is. To illustrate this notion, we need to take into account its distinct measurements from different observational missions. The estimation of H_0 by the Planck 2015 missions from the ΛCDM-based cosmological model yields $H_0 = 67.27 \pm 0.66$ km/s/Mpc (Planck TT, TE, EE + lowP) [1], while the local measurement of H_0 using the Hubble Space Telescope gives $H_0 = 73.24 \pm 1.74$ km/s/Mpc [85]: this huge difference between these estimations is generally known as the tension on the Hubble constant. Some recent investigations have already shown that interacting dark energy might be able to release such tension on H_0 [20,94]. Since interacting dark energy is purely model dependent, it is naturally quite justified to wonder how other phenomenological interaction models react with the tension on H_0. To make this more clear, in Table V we summarize the constraints on H_0 for both IDE and IVS up to the 3σ confidence level. We see that the addition of one extra

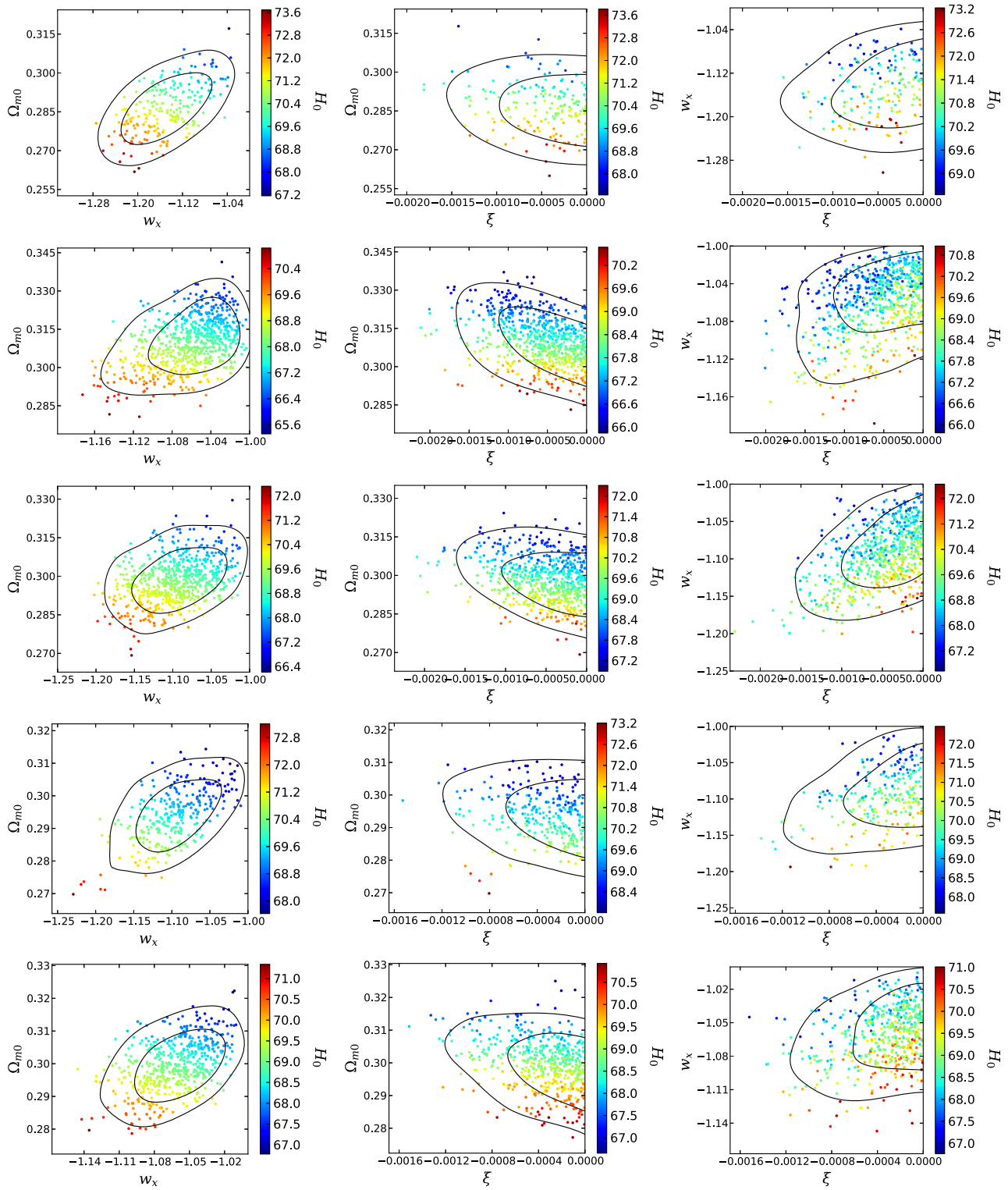

FIG. 13. In each panel we show three-dimensional scatter plots colored by the H_0 values of the MCMC chains of the corresponding combined analysis. The combined analyses from top to bottom are (i) CMB + BAO + HST, (ii) CMB + BAO + RSD, (iii) CMB + BAO + RSD + HST, (iv) CMB + BAO + RSD + HST + JLA + CC, and (v) CMB + BAO + RSD + HST + JLA+ CC + WL. First column: From the MCMC chains of all combined analyses, we notice that as the values of H_0 decrease (represented by the points in blue) the dark energy equation of state moves toward the cosmological constant boundary. Second column: The MCMC chains of all combined analyses infer that the lower values of H_0 prefer a nonzero coupling in the dark sector, which is statistically consistent with zero. Last column: With lower values of H_0, the dark energy equation of state moves toward the cosmological constant boundary and a nonzero coupling in the dark sector is favored, which is indeed very close to zero.

TABLE III. The $\chi^2_{\rm min}$ obtained for the best-fit values of the parameters of the two interacting dark energy scenarios and noninteracting ΛCDM cosmology.

Model	CMB	CMB + BAO +HST	CMB + BAO +RSD	CMB + BAO +RSD + HST	CMB + BAO +RSD + HST +JLA + CC	CMB + BAO +RSD + HST +JLA + CC + WL
IDE: $\chi^2_{\rm min}$ (best-fit)	12 960.778	12 981.276	12 975.450	12 982.168	13 689.092	13 723.708
IVS: $\chi^2_{\rm min}$ (best-fit)	12 961.606	12 980.844	12 971.080	12 982.742	13 693.894	13 724.124
ΛCDM: $\chi^2_{\rm min}$ (best-fit)	12 964.062	12 978.886	12 974.124	12 981.336	13 693.560	13 722.170

degree of freedom (d.o.f.) in terms of the coupling parameter significantly increases the error bars on H_0 compared to Planck 2015 [1]. And the increase of error bars on H_0 is prominent for IDE compared to IVS because the estimated values of H_0 for IVS using different combined analyses look similar to Planck 2015 [1]. Naturally, for the IDE scenario one may infer that, due to the large error bars present on H_0, the estimated values of H_0 are in agreement with the local measurement ($H_0 = 73.24 \pm 1.74$ km/s/Mpc) [85]. Thus, one can see that the interaction in the dark sector may provide a way to reduce the tension on H_0.

D. The Bayesian evidence

Model selection [98] plays an important role in distinguishing various cosmological models. Keeping the same motivation, in this work we compare both interacting dark energy scenarios with the ΛCDM cosmological model using Bayesian analysis. The Bayesian evidence is a powerful statistical technique that quantifies the cosmological models based on their performance with the observational data. In the following, we briefly describe how the Bayesian evidence is calculated for a cosmological model. In the Bayesian analysis one needs the posterior probability of the model parameters (denoted by θ), given a particular data set x to test the model, any prior information, and a model M. Now, recalling Bayes theorem, one may write

$$p(\theta|x, M) = \frac{p(x|\theta, M)\pi(\theta|M)}{p(x|M)}, \tag{37}$$

where $p(x|\theta, M)$ is the likelihood function dependent on the model parameters θ with the data set fixed; $\pi(\theta|M)$ is the prior used in the analysis. The denominator $p(x|M)$ on the right-hand side of Eq. (37) is the Bayesian evidence for the model comparison and it is the integral over the un-normalized posterior $\tilde{p}(\theta|x, M) \equiv p(x|\theta, M)\pi(\theta|M)$,

$$E \equiv p(x|M) = \int d\theta p(x|\theta, M)\pi(\theta|M). \tag{38}$$

We note that Eq. (38) is also referred to as the marginal likelihood. Now, for any particular model M_i and the reference model M_j (the base model, here ΛCDM), the posterior probability is given by

TABLE IV. The observational constraints of the cosmological parameters for the IVS at the 68.3% confidence level for different combinations of observational data. For the coupling parameter ξ, we report only values at the 95.4% lower confidence level.

Parameters	CMB	CMB + BAO +HST	CMB + BAO +RSD	CMB + BAO +RSD + HST	CMB + BAO +RSD + HST +JLA + CC	CMB + BAO +RSD + HST +JLA + CC + WL
$\Omega_c h^2$	$0.1225^{+0.0021}_{-0.0031}$	$0.1178^{+0.0010}_{-0.0010}$	$0.1193^{+0.0011}_{-0.0011}$	$0.1183^{+0.0011}_{-0.0012}$	$0.1182^{+0.0011}_{-0.0011}$	$0.1178^{+0.0010}_{-0.0010}$
$\Omega_b h^2$	$0.0223^{+0.0002}_{-0.0002}$	$0.0224^{+0.0001}_{-0.0001}$	$0.0223^{+0.0001}_{-0.0001}$	$0.0224^{+0.0002}_{-0.0001}$	$0.0224^{+0.0001}_{-0.0001}$	$0.0224^{+0.0001}_{-0.0001}$
$100\theta_{MC}$	$1.0402^{+0.0004}_{-0.0004}$	$1.0408^{+0.0003}_{-0.0003}$	$1.0405^{+0.0003}_{-0.0003}$	$1.0407^{+0.0003}_{-0.0003}$	$1.0407^{+0.0003}_{-0.0004}$	$1.0407^{+0.0003}_{-0.0003}$
τ	$0.0765^{+0.0192}_{-0.0178}$	$0.0915^{+0.0185}_{-0.0155}$	$0.0781^{+0.0138}_{-0.0157}$	$0.0796^{+0.0165}_{-0.0163}$	$0.0793^{+0.0156}_{-0.0162}$	$0.0750^{+0.0169}_{-0.0160}$
n_s	$0.9695^{+0.0048}_{-0.0049}$	$0.9788^{+0.0037}_{-0.0038}$	$0.9750^{+0.0035}_{-0.0036}$	$0.9771^{+0.0039}_{-0.0038}$	$0.9773^{+0.0039}_{-0.0041}$	$0.9783^{+0.0035}_{-0.0038}$
$\ln(10^{10}A_s)$	$3.0966^{+0.0373}_{-0.0339}$	$3.1214^{+0.0373}_{-0.0311}$	$3.0960^{+0.0275}_{-0.0283}$	$3.0979^{+0.0311}_{-0.0319}$	$3.0965^{+0.0316}_{-0.0350}$	$3.0863^{+0.0327}_{-0.0316}$
Ω_{m0}	$0.3425^{+0.0159}_{-0.0271}$	$0.3064^{+0.0063}_{-0.0064}$	$0.3167^{+0.0074}_{-0.0071}$	$0.3096^{+0.0068}_{-0.0077}$	$0.30911013^{+0.0065}_{-0.0077}$	$0.3064^{+0.0061}_{-0.0065}$
σ_8	$0.8118^{+0.0212}_{-0.0170}$	$0.8262^{+0.0156}_{-0.0127}$	$0.8169^{+0.0120}_{-0.0120}$	$0.8167^{+0.0124}_{-0.0125}$	$0.8161^{+0.0134}_{-0.0143}$	$0.8108^{+0.0128}_{-0.0127}$
H_0	$65.2375^{+1.8234}_{-1.1629}$	$67.8090^{+0.5004}_{-0.4817}$	$67.0308^{+0.5368}_{-0.5437}$	$67.5675^{+0.5413}_{-0.5259}$	$67.6067^{+0.5796}_{-0.5032}$	$67.7953^{+0.4983}_{-0.4735}$
ξ	$\xi > -0.001953$	$\xi > -0.000490$	$\xi > -0.000726$	$\xi > -0.000549$	$\xi > -0.000563$	$\xi > -0.000557$

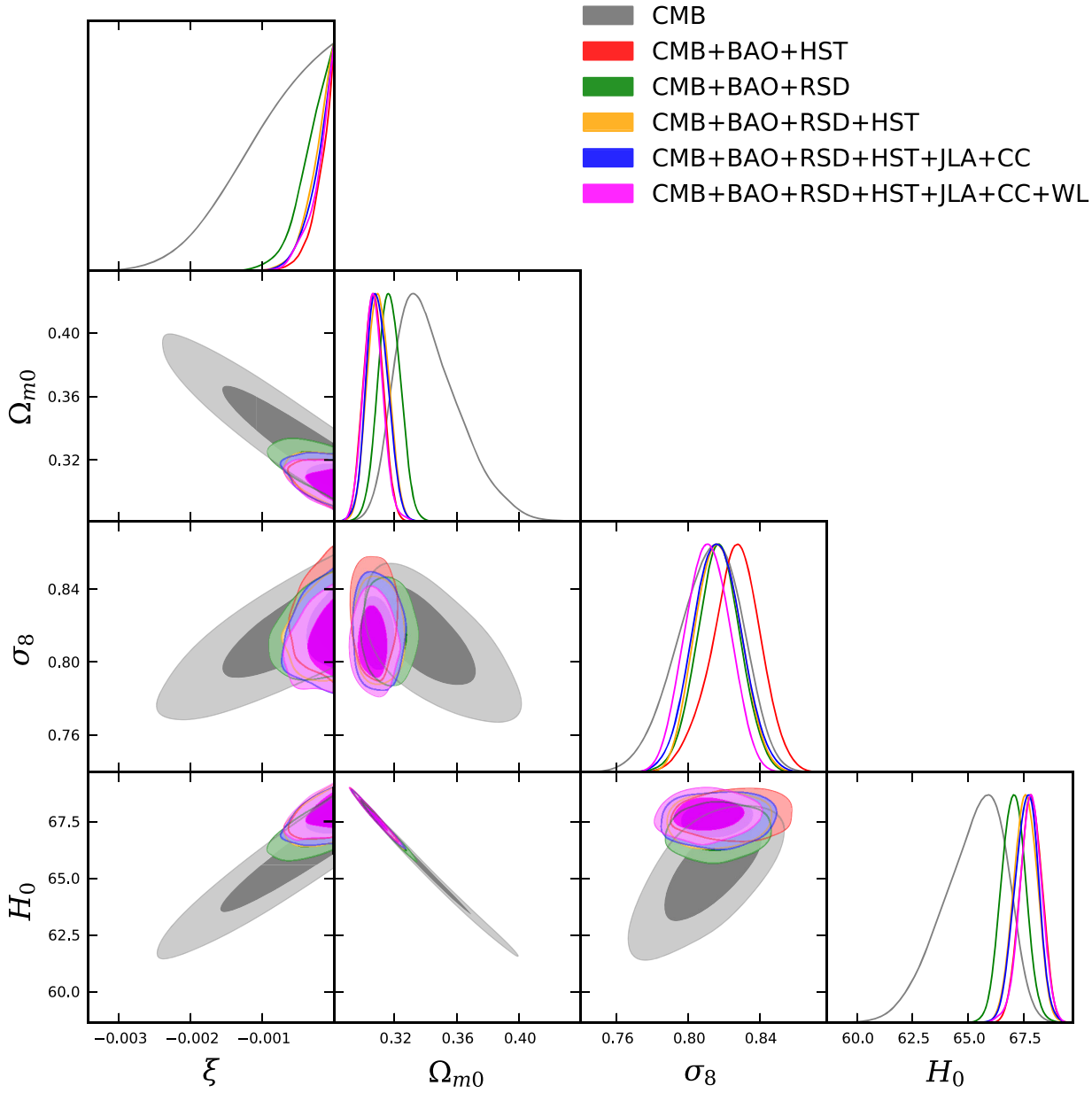

FIG. 14. Contour plots for different combinations of the cosmological parameters at the 68.3% and 95.4% confidence levels for the IVS are shown for distinct observational combinations. Additionally, we also show the one-dimensional posterior distributions for those parameters at the extreme right corners of each row. From the two-dimensional contour plots one can see that the addition of any external data to CMB decreases the error bars of the cosmological parameters.

$$\frac{p(M_i|x)}{p(M_j|x)} = \frac{\pi(M_i)}{\pi(M_j)}\frac{p(x|M_i)}{p(x|M_j)} = \frac{\pi(M_i)}{\pi(M_j)}B_{ij}, \qquad (39)$$

where $B_{ij} = \frac{p(x|M_i)}{p(x|M_j)}$ is the Bayes factor of the model M_i relative to the base or reference model M_j. For $B_{ij} > 1$, the data support the model M_i more strongly than the model M_j. The behavior of the models is usually quantified using different values of B_{ij} (or, alternatively, $\ln B_{ij}$). Here, we shall use the widely accepted Jeffreys scales [99] (see Table VI) that summarizes the model comparison.

Now, one can calculate the Bayesian evidence using the MCMC chains which directly extract the parameters of the underlying cosmological model. For a detailed explanation of the implementation of the Bayesian evidence for any cosmological model, we refer to Refs. [100,101] where we used the code MCEVIDENCE.[1]

[1]This code is available for free at https://github.com/yabebalFantaye/MCEvidence.

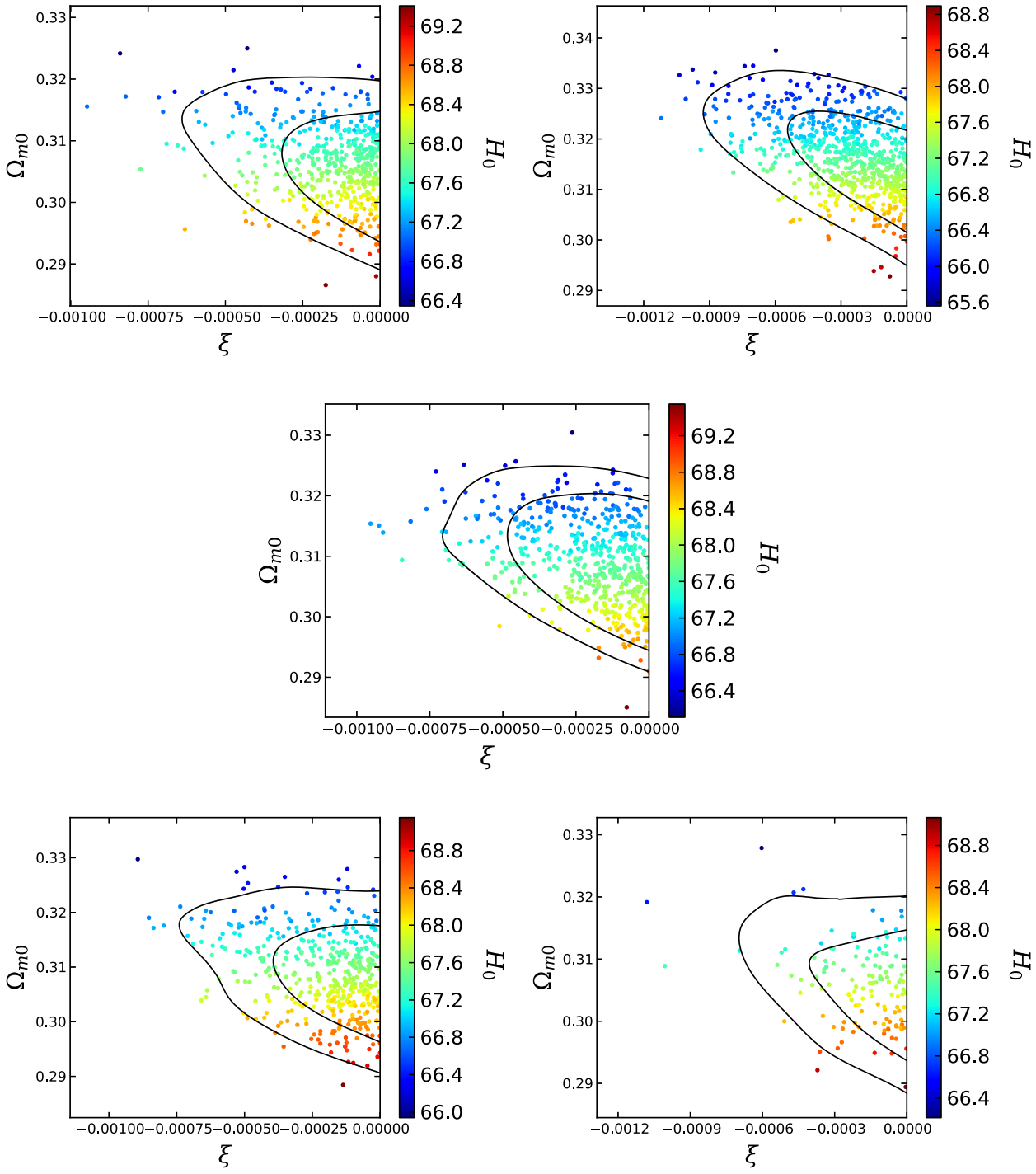

FIG. 15. For the interacting vacuum scenario, we analyze the MCMC chains of the combined analysis in the two-dimensional (ξ, Ω_{m0}) plane colored by the Hubble parameter values. The upper left and upper right panels, respectively, represent the analyses CMB + BAO + HST and CMB + BAO + RSD. The center plot shows the combined analysis CMB + BAO + RSD + HST. Finally, the lower left and lower right panels, respectively, represent the analyses CMB + BAO + RSD + HST + JLA + CC and CMB + BAO + RSD + HST + JLA + CC + WL. From all of the plots one thing is clear: lower values of the Hubble parameter signal a nonzero interaction in the dark sector, while statistically this is consistent with zero and, in addition, the density parameter for the matter sector is also allowed to take higher values.

TABLE V. The 68%, 95%, and 99% confidence-level constraints on H_0 and σ_8 for different combined analyses for the interacting scenario with $w_x < -1$ (IDE) and $w_x = -1$ (IVS). We note that the estimation of H_0 by the latest Planck missions for the base ΛCDM model yields $H_0 = 67.27 \pm 0.66$ km/s/Mpc (Planck TT, TE, EE + lowP) [1].

Parameter	CMB	CMB + BAO +HST	CMB + BAO +RSD	CMB + BAO +RSD + HST	CMB + BAO +RSD + HST +JLA + CC	CMB + BAO +RSD + HST +JLA + CC + WL
H_0 (IDE)	$65.52^{+4.51+7.53+9.45}_{-3.93-8.02-10.22}$	$70.77^{+1.11+2.31+2.78}_{-1.15-2.32-2.47}$	$67.97^{+0.83+1.86+2.56}_{-1.02-1.77-2.05}$	$69.19^{+0.87+1.79+2.46}_{-0.89-1.72-2.22}$	$69.64^{+0.83+1.69+2.79}_{-0.85-1.75-2.20}$	$68.89^{+0.68+1.52+1.93}_{-0.82-1.36-1.88}$
H_0 (IVS)	$65.24^{+1.82+2.67+3.21}_{-1.16-3.06-4.14}$	$67.81^{+0.50+0.97+1.17}_{-0.48-0.98-1.24}$	$67.03^{+0.54+1.08+1.46}_{-0.54-1.09-1.41}$	$67.57^{+0.54+0.96+1.31}_{-0.53-1.01-1.35}$	$67.61^{+0.58+0.98+1.39}_{-0.50-1.03-1.34}$	$67.80^{+0.50+1.06+1.23}_{-0.47-1.04-1.54}$

Thus, using the code MCEVIDENCE, we calculate the logarithm of the Bayes factor, i.e., $\ln B_{ij}$ where i stands for IDE or IVS and j is the reference model (ΛCDM). In Table VII we show the calculated values of $\ln B_{ij}$ for the two interacting scenarios with respect to ΛCDM. From the table, we see that for all of the observational data employed in this work, the values of $\ln B_{ij}$ are negative, which from the point of view of the Bayesian evidence shows that the reference model (ΛCDM) is preferred over the two interacting scenarios. For some combined analyses the preference for ΛCDM is strong, while for others it is positive. Overall, we see that the present observational data always favors ΛCDM with respect to the interacting scenarios discussed in this work.

TABLE VI. Revised Jeffreys scale used to test the observational support of any model M_i with respect to another model M_j.

$\ln B_{ij}$	Strength of evidence for model M_i
$0 \leq \ln B_{ij} < 1$	Weak
$1 \leq \ln B_{ij} < 3$	Definite/Positive
$3 \leq \ln B_{ij} < 5$	Strong
$\ln B_{ij} \geq 5$	Very strong

VI. CONCLUDING REMARKS

We have considered an interacting scenario between a pressureless dark matter and a dark energy fluid with a constant barotropic equation of state. The underlying geometry of the universe is characterized by the spatially flat FLRW line element, and the interaction rate $Q = Q(\rho_t') = Q(\rho_c, \rho_x)$ has been given explicitly in Eq. (8) or Eq. (9). This interaction rate is very appealing in the sense that the evolution equations for the dark sectors (cold dark matter and dark energy) can be exactly solved, and thus, one can directly measure their deviation from the standard evolution laws of the dark fluids with no interaction. We note that initially this kind of interaction was introduced by Chimento in Ref. [30], where the author proposed a very general interaction rate that recovers the interaction in Eq. (9) and discussed its theoretical implications. Later, its observational viability was tested with dark energy as the cosmological constant but at the background level [42]; consequently, in a recent article [61], the authors generalized this study for both $w_x = -1$ and $w_x \neq -1$ at the background level with recent observational data. However, it is quite certain that the dynamics of such interaction models on large scales is a promising tool to better understand the entire scenario. This means that the most

TABLE VII. Summary of $\ln B_{ij}$, for the two interacting scenarios with respect to the reference model ΛCDM, for different observational data sets. From the Bayesian evidence point of view, negative values of $\ln B_{ij}$ mean that the reference model ΛCDM is preferred over the two interacting scenarios.

Data set	Model	$\ln B_{ij}$	Strength of evidence for ΛCDM
CMB	IDE	−2.0	Positive
CMB	IVS	−1.9	Positive
CMB + BAO + HST	IDE	−4.8	Strong
CMB + BAO + HST	IVS	−3.5	Strong
CMB + BAO + RSD	IDE	−2.9	Positive
CMB + BAO + RSD	IVS	−1.7	Positive
CMB + BAO + RSD + HST	IDE	−3.6	Strong
CMB + BAO + RSD + HST	IVS	−3.3	Strong
CMB + BAO + RSD + HST + JLA + CC	IDE	−1.7	Positive
CMB + BAO + RSD + HST + JLA + CC	IVS	−2.2	Positive
CMB + BAO + RSD + HST + JLA + CC + WL	IDE	−4.0	Strong
CMB + BAO + RSD + HST + JLA + CC + WL	IVS	−3.7	Strong

important question related to the interaction model is how the structure formation of the Universe changes when such an interaction is included in the cosmological scenario. Thus, in the present work we discussed the perturbations and structure formation of the Universe when such an interaction is present between the dark fluids. Now, in order to test the resulting cosmological scenarios with the available observational data, we used CosmoMC, a Markov chain Monte Carlo package that extracts the model parameters with a sufficient convergence following the Gelman-Rubin statistics [92]. The observational data include cosmic microwave background radiation, baryon acoustic oscillations, redshift-space distortions, the local Hubble constant, supernovae type Ia data from joint light curve analysis, Hubble parameter values at different redshifts from cosmic chronometers, and finally weak gravitational lensing data. For a better analysis, we have considered two distinct interacting scenarios, namely, when the dark energy is and is not (i.e., $w_x \neq -1$) the cosmological constant.

For the IDE scenario, the constraints on the model parameters are summarized in Table II where we presented the 95.4% (lower) confidence limits on the coupling parameter ξ. In Fig. 9, we showed the contour plots for different combinations of model parameters at the 68.3% and 95.4% confidence levels. The right corners of Fig. 9 also show the one-dimensional posterior distributions for some selected model parameters. From the observational constraints on the coupling parameter ξ, summarized in the last row of Table II, we find that $\xi = 0$ is consistent with the observational data. Moreover, from the constraints on the dark energy equation of state w_x, one can see that it is actually very close to the cosmological constant boundary. Thus, we see that the interaction model is actually equivalent to the noninteracting ΛCDM background. However, in the large-scale distribution, the interaction model may exhibit some differences even for a very small coupling strength. From the imprints on the CMB TT spectra (see the right panel of Fig. 1) and also from the matter power spectra (see the right panel of Fig. 2), it is evident that for a very small coupling strength ($\xi = -0.0001$), the model presents a very minimal deviation from the noninteracting ΛCDM cosmology.

The results for the interacting cosmological constant (IVS) are summarized in Table IV. The corresponding contour plots at the 68.3% and 95.4% confidence levels are also shown in Fig. 14 with the one-dimensional posterior distributions for some selected parameters of this model. From the estimation of the coupling strength shown in Table IV, one can see that ξ is consistent with the noninteraction limit (i.e., $\xi = 0$), at least according to the current observational data. In fact, for this model we have realized a similar trend as in IDE. For instance, from Fig. 15, similar to the IDE model, we found that lower values of the Hubble parameter allow nonzero interaction in the dark sector. The deviation of this interaction scenario from the noninteracting ΛCDM cosmology is also found to be insensitive (see the right panels of Figs. 5 and 6), unlike the IDE scenario where (although small) the deviation is detectable.

We also addressed one interesting point that has become a hot issue in current cosmological research: the observed tension on H_0 between its global [1] and local measurements [85]. We found that the allowance of the interaction increases the error bars on the Hubble parameter measurements, and consequently, the parameter space for H_0 is increased. This effectively partially releases the tension and is reflected in some combinations for IDE only, while the interacting vacuum model is not suitable to release the tension. One may argue that the allowance of extra d.o.f. in the parameter space of the interacting dark energy models (for IDE the number of parameters is eight, while for IVS it is seven) might be suitable to alleviate such tension. Similar results have been reported in some recent works [20,94]; however, since the theory of interaction is phenomenological and hence its conclusions are as well, an analysis with a different interaction model might be important to see whether the model can alleviate this tension. The relation between the extra d.o.f. and the tension on H_0 in the interacting dark energy models surely needs further attention.

Finally, we computed the Bayesian evidence for each interacting scenario with respect to the noninteracting ΛCDM model (see Table VII). Our analysis shows that the noninteracting ΛCDM is preferred over the two interacting dark energy scenarios, at least according to the current observational data sets.

ACKNOWLEDGMENTS

The authors thank the referee for his/her constructive and illuminating comments that improved the work considerably. W. Y. is supported by the National Natural Science Foundation of China under Grants No. 11705079 and No. 11647153. R. H. was supported by Proyecto VRIEA-PUCV No. 039.309/2018. S. C. acknowledges the financial support from the Mathematical Research Impact Centric Support (MATRICS), Project Reference No. MTR/2017/000407, by the Science and Engineering Research Board, Government of India. S. P. thanks Rafael C. Nunes, Burin Gumjudpai, and J. A. S. Lima for useful discussions and comments while working on the draft.

[1] P. A. R. Ade *et al.* (Planck Collaboration), Planck 2015 results. XIII. Cosmological parameters, Astron. Astrophys. **594**, A13 (2016).

[2] S. Weinberg, The cosmological constant problem, Rev. Mod. Phys. **61**, 1 (1989).

[3] C. Wetterich, An asymptotically vanishing time-dependent cosmological "constant", Astron. Astrophys. **301**, 321 (1995).

[4] E. J. Copeland, M. Sami, and S. Tsujikawa, Dynamics of dark energy, Int. J. Mod. Phys. D **15**, 1753 (2006).

[5] L. Amendola and S. Tsujikawa, *Dark Energy: Theory and Observations* (Cambridge University Press, Cambridge, England, 2010).

[6] K. Bamba, S. Capozziello, S. Nojiri, and S. D. Odintsov, Dark energy cosmology: The equivalent description via different theoretical models and cosmography tests, Astrophys. Space Sci. **342**, 155 (2012).

[7] I. Zlatev, L. M. Wang, and P. J. Steinhardt, Quintessence, cosmic coincidence, and the cosmological constant, Phys. Rev. Lett. **82**, 896 (1999).

[8] L. Amendola, Coupled quintessence, Phys. Rev. D **62**, 043511 (2000).

[9] L. P. Chimento, A. S. Jakubi, D. Pavón, and W. Zimdahl, Interacting quintessence solution to the coincidence problem, Phys. Rev. D **67**, 083513 (2003).

[10] R. G. Cai and A. Wang, Cosmology with interaction between phantom dark energy and dark matter and the coincidence problem, J. Cosmol. Astropart. Phys. 03 (2005) 002.

[11] B. Hu and Y. Ling, Interacting dark energy, holographic principle and coincidence problem, Phys. Rev. D **73**, 123510 (2006).

[12] S. del Campo, R. Herrera, and D. Pavón, Toward a solution of the coincidence problem, Phys. Rev. D **78**, 021302 (2008).

[13] S. del Campo, R. Herrera, and D. Pavón, Interacting models may be key to solve the cosmic coincidence problem, J. Cosmol. Astropart. Phys. 01 (2009) 020.

[14] V. Salvatelli, N. Said, M. Bruni, A. Melchiorri, and D. Wands, Indications of a late-time interaction in the dark sector, Phys. Rev. Lett. **113**, 181301 (2014).

[15] R. C. Nunes, S. Pan, and E. N. Saridakis, New constraints on interacting dark energy from cosmic chronometers, Phys. Rev. D **94**, 023508 (2016).

[16] S. Kumar and R. C. Nunes, Probing the interaction between dark matter and dark energy in the presence of massive neutrinos, Phys. Rev. D **94**, 123511 (2016).

[17] W. Yang, H. Li, Y. Wu, and J. Lu, Cosmological constraints on coupled dark energy, J. Cosmol. Astropart. Phys. 10 (2016) 007.

[18] C. van de Bruck, J. Mifsud, and J. Morrice, Testing coupled dark energy models with their cosmological background evolution, Phys. Rev. D **95**, 043513 (2017).

[19] W. Yang, N. Banerjee, and S. Pan, Constraining a dark matter and dark energy interaction scenario with a dynamical equation of state, Phys. Rev. D **95**, 123527 (2017).

[20] S. Kumar and R. C. Nunes, Echo of interactions in the dark sector, Phys. Rev. D **96**, 103511 (2017).

[21] W. Yang, S. Pan, and J. D. Barrow, Large-scale stability and astronomical constraints for coupled dark-energy models, Phys. Rev. D **97**, 043529 (2018).

[22] S. Kumar and R. C. Nunes, Observational constraints on dark matter–dark energy scattering cross section, Eur. Phys. J. C **77**, 734 (2017).

[23] W. Yang, S. Pan, and D. F. Mota, Novel approach toward the large-scale stable interacting dark-energy models and their astronomical bounds, Phys. Rev. D **96**, 123508 (2017).

[24] A. P. Billyard and A. A. Coley, Interactions in scalar field cosmology, Phys. Rev. D **61**, 083503 (2000).

[25] B. Gumjudpai, T. Naskar, M. Sami, and S. Tsujikawa, Coupled dark energy: Towards a general description of the dynamics, J. Cosmol. Astropart. Phys. 06 (2005) 007.

[26] J. D. Barrow and T. Clifton, Cosmologies with energy exchange, Phys. Rev. D **73**, 103520 (2006).

[27] W. Zimdahl and D. Pavón, Interacting holographic dark energy, Classical Quantum Gravity **24**, 5461 (2007).

[28] L. Amendola, G. C. Campos, and R. Rosenfeld, Consequences of dark matter–dark energy interaction on cosmological parameters derived from SNIa data, Phys. Rev. D **75**, 083506 (2007).

[29] G. Caldera-Cabral, R. Maartens, and L. A. Ureña-López, Dynamics of interacting dark energy, Phys. Rev. D **79**, 063518 (2009).

[30] L. P. Chimento, Linear and nonlinear interactions in the dark sector, Phys. Rev. D **81**, 043525 (2010).

[31] M. Quartin, M. O. Calvao, S. E. Joras, R. R. R. Reis, and I. Waga, Dark interactions and cosmological fine-tuning, J. Cosmol. Astropart. Phys. 05 (2008) 007.

[32] J. Väliviita, R. Maartens, and E. Majerotto, Observational constraints on an interacting dark energy model, Mon. Not. R. Astron. Soc. **402**, 2355 (2010).

[33] T. Clemson, K. Koyama, G. B. Zhao, R. Maartens, and J. Valiviita, Interacting dark energy: Constraints and degeneracies, Phys. Rev. D **85**, 043007 (2012).

[34] M. Thorsrud, D. F. Mota, and S. Hervik, Cosmology of a scalar field coupled to matter and an isotropy-violating Maxwell field, J. High Energy Phys. 10 (2012) 066.

[35] S. Pan and S. Chakraborty, Will there be again a transition from acceleration to deceleration in course of the dark energy evolution of the universe?, Eur. Phys. J. C **73**, 2575 (2013).

[36] W. Yang and L. Xu, Coupled dark energy with perturbed Hubble expansion rate, Phys. Rev. D **90**, 083532 (2014).

[37] V. Faraoni, J. B. Dent, and E. N. Saridakis, Covariantizing the interaction between dark energy and dark matter, Phys. Rev. D **90**, 063510 (2014).

[38] W. Yang and L. Xu, Cosmological constraints on interacting dark energy with redshift-space distortion after Planck data, Phys. Rev. D **89**, 083517 (2014).

[39] R. C. Nunes and E. M. Barboza, Dark matter-dark energy interaction for a time-dependent EoS parameter, Gen. Relativ. Gravit. **46**, 1820 (2014).

[40] S. Pan and S. Chakraborty, A cosmographic analysis of holographic dark energy models, Int. J. Mod. Phys. D **23**, 1450092 (2014).

[41] X. m. Chen, Y. Gong, E. N. Saridakis, and Y. Gong, Time-dependent interacting dark energy and transient acceleration, Int. J. Theor. Phys. **53**, 469 (2014).

[42] I. E. Sanchez G., Dark matter interacts with variable vacuum energy, Gen. Relativ. Gravit. **46**, 1769 (2014).

[43] S. Pan, S. Bhattacharya, and S. Chakraborty, An analytic model for interacting dark energy and its observational constraints, Mon. Not. R. Astron. Soc. **452**, 3038 (2015).
[44] Y. H. Li and X. Zhang, Large-scale stable interacting dark energy model: Cosmological perturbations and observational constraints, Phys. Rev. D **89**, 083009 (2014).
[45] D. G. A. Duniya, D. Bertacca, and R. Maartens, Probing the imprint of interacting dark energy on very large scales, Phys. Rev. D **91**, 063530 (2015).
[46] J. Väliviita and E. Palmgren, Distinguishing interacting dark energy from *w*CDM with CMB, lensing, and baryon acoustic oscillation data, J. Cosmol. Astropart. Phys. 07 (2015) 015.
[47] J. Solà, J. de Cruz Pérez, and A. Gómez-Valent, Dynamical dark energy versus $\Lambda = \text{const}$ in light of observations, Europhys. Lett. **121**, 39001 (2018).
[48] A. Mukherjee and N. Banerjee, In search of the dark matter dark energy interaction: A kinematic approach, Classical Quantum Gravity **34**, 035016 (2017).
[49] S. Pan and G. S. Sharov, A model with interaction of dark components and recent observational data, Mon. Not. R. Astron. Soc. **472**, 4736 (2017).
[50] J. Dutta, W. Khyllep, and N. Tamanini, Scalar-fluid interacting dark energy: Cosmological dynamics beyond the exponential potential, Phys. Rev. D **95**, 023515 (2017).
[51] R. G. Cai, N. Tamanini, and T. Yang, Reconstructing the dark sector interaction with LISA, J. Cosmol. Astropart. Phys. 05 (2017) 031.
[52] S. D. Odintsov, V. K. Oikonomou, and P. V. Tretyakov, Phase space analysis of the accelerating multifluid Universe, Phys. Rev. D **96**, 044022 (2017).
[53] S. Pan, A. Mukherjee, and N. Banerjee, Astronomical bounds on a cosmological model allowing a general interaction in the dark sector, Mon. Not. R. Astron. Soc. **477**, 1189 (2018).
[54] W. Yang, S. Pan, and A. Paliathanasis, Cosmological constraints on an exponential interaction in the dark sector, arXiv:1804.08558.
[55] W. Yang, S. Pan, L. Xu, and D. F. Mota, Effects of anisotropic stress in interacting dark matter–dark energy scenarios, arXiv:1804.08455.
[56] W. Yang, S. Pan, E. Di Valentino, R. C. Nunes, S. Vagnozzi, and D. F. Mota, Tale of stable interacting dark energy, observational signatures, and the H_0 tension, arXiv:1805.08252.
[57] Y. L. Bolotin, A. Kostenko, O. A. Lemets, and D. A. Yerokhin, Cosmological evolution with interaction between dark energy and dark matter, Int. J. Mod. Phys. D **24**, 1530007 (2015).
[58] B. Wang, E. Abdalla, F. Atrio-Barandela, and D. Pavón, Dark matter and dark energy interactions: Theoretical challenges, cosmological implications and observational signatures, Rep. Prog. Phys. **79**, 096901 (2016).
[59] G. Izquierdo, R. C. Blanquet-Jaramillo, and R. A. Sussman, Dynamics of a spherically symmetric inhomogeneous coupled dark energy model with coupling term proportional to nonrelativistic matter, Gen. Relativ. Gravit. **50**, 2 (2018).
[60] G. Izquierdo, R. C. Blanquet-Jaramillo, and R. A. Sussman, Interactive mixture of inhomogeneous dark fluids driven by dark energy: A dynamical system analysis, Eur. Phys. J. C **78**, 233 (2018).
[61] G. S. Sharov, S. Bhattacharya, S. Pan, R. C. Nunes, and S. Chakraborty, A new interacting two fluid model and its consequences, Mon. Not. R. Astron. Soc. **466**, 3497 (2017).
[62] C. G. Park, J. c. Hwang, J. h. Lee, and H. Noh, Roles of dark energy perturbations in the dynamical dark energy models: Can we ignore them?, Phys. Rev. Lett. **103**, 151303 (2009).
[63] R. Bean and O. Dore, Probing dark energy perturbations: The dark energy equation of state and speed of sound as measured by WMAP, Phys. Rev. D **69**, 083503 (2004).
[64] J. Weller and A. M. Lewis, Large scale cosmic microwave background anisotropies and dark energy, Mon. Not. R. Astron. Soc. **346**, 987 (2003).
[65] T. Koivisto, Growth of perturbations in dark matter coupled with quintessence, Phys. Rev. D **72**, 043516 (2005).
[66] R. Bean, E. E. Flanagan, and M. Trodden, Adiabatic instability in coupled dark energy-dark matter models, Phys. Rev. D **78**, 023009 (2008).
[67] R. Herrera, W. S. Hipolito-Ricaldi, and N. Videla, Instability in interacting dark sector: An appropriate holographic Ricci dark energy model, J. Cosmol. Astropart. Phys. 08 (2016) 065.
[68] S. del Campo, J. C. Fabris, R. Herrera, and W. Zimdahl, Cosmology with Ricci dark energy, Phys. Rev. D **87**, 123002 (2013).
[69] J. Väliviita, E. Majerotto, and R. Maartens, Instability in interacting dark energy and dark matter fluids, J. Cosmol. Astropart. Phys. 07 (2008) 020.
[70] M. S. Turner, Coherent scalar field oscillations in an expanding Universe, Phys. Rev. D **28**, 1243 (1983).
[71] K. A. Malik, D. Wands, and C. Ungarelli, Large scale curvature and entropy perturbations for multiple interacting fluids, Phys. Rev. D **67**, 063516 (2003).
[72] V. F. Mukhanov, H. A. Feldman, and R. H. Brandenberger, Theory of cosmological perturbations, Phys. Rep. **215**, 203 (1992).
[73] C. P. Ma and E. Bertschinger, Cosmological perturbation theory in the synchronous and conformal Newtonian gauges, Astrophys. J. **455**, 7 (1995).
[74] K. A. Malik and D. Wands, Cosmological perturbations, Phys. Rep. **475**, 1 (2009).
[75] E. Majerotto, J. Valiviita, and R. Maartens, Adiabatic initial conditions for perturbations in interacting dark energy models, Mon. Not. R. Astron. Soc. **402**, 2344 (2010).
[76] K. Koyama, R. Maartens, and Y. S. Song, Velocities as a probe of dark sector interactions, J. Cosmol. Astropart. Phys. 10 (2009) 017.
[77] W. Hu, Structure formation with generalized dark matter, Astrophys. J. **506**, 485 (1998).
[78] H. Kodama and M. Sasaki, Cosmological perturbation theory, Prog. Theor. Phys. Suppl. **78**, 1 (1984).
[79] R. Adam *et al.* (Planck Collaboration), Planck 2015 results. I. Overview of products and scientific results, Astron. Astrophys. **594**, A1 (2016).
[80] N. Aghanim *et al.* (Planck Collaboration), Planck 2015 results. XI. CMB power spectra, likelihoods, and robustness of parameters, Astron. Astrophys. **594**, A11 (2016).
[81] F. Beutler, C. Blake, M. Colless, D. H. Jones, L. Staveley-Smith, L. Campbell, Q. Parker, W. Saunders, and

F. Watson, The 6dF Galaxy Survey: Baryon acoustic oscillations and the local Hubble constant, Mon. Not. R. Astron. Soc. **416**, 3017 (2011).

[82] A. J. Ross, L. Samushia, C. Howlett, W. J. Percival, A. Burden, and M. Manera, The clustering of the SDSS DR7 main Galaxy sample—I: A 4 per cent distance measure at $z = 0.15$, Mon. Not. R. Astron. Soc. **449**, 835 (2015).

[83] H. Gil-Marín *et al.*, The clustering of galaxies in the SDSS-III Baryon Oscillation Spectroscopic Survey: BAO measurement from the LOS-dependent power spectrum of DR12 BOSS galaxies, Mon. Not. R. Astron. Soc. **460**, 4210 (2016).

[84] H. Gil-Marín, W. J. Percival, L. Verde, J. R. Brownstein, C.-H. Chuang, F.-S. Kitaura, S. A. Rodríguez-Torres, and M. D. Olmstead, The clustering of galaxies in the SDSS-III Baryon Oscillation Spectroscopic Survey: RSD measurement from the power spectrum and bispectrum of the DR12 BOSS galaxies, Mon. Not. R. Astron. Soc. **465**, 1757 (2017).

[85] A. G. Riess *et al.*, A 2.4% determination of the local value of the Hubble constant, Astrophys. J. **826**, 56 (2016).

[86] M. Betoule *et al.* (SDSS Collaboration), Improved cosmological constraints from a joint analysis of the SDSS-II and SNLS supernova samples, Astron. Astrophys. **568**, A22 (2014).

[87] M. Moresco, L. Pozzetti, A. Cimatti, R. Jimenez, C. Maraston, L. Verde, D. Thomas, A. Citro, R. Tojeiro, and D. Wilkinson, A 6% measurement of the Hubble parameter at $z \sim 0.45$: Direct evidence of the epoch of cosmic re-acceleration, J. Cosmol. Astropart. Phys. 05 (2016) 014.

[88] C. Heymans *et al.*, CFHTLenS tomographic weak lensing cosmological parameter constraints: Mitigating the impact of intrinsic galaxy alignments, Mon. Not. R. Astron. Soc. **432**, 2433 (2013).

[89] M. Asgari, C. Heymans, C. Blake, J. Harnois-Deraps, P. Schneider, and L. Van Waerbeke, Revisiting CFHTLenS cosmic shear: Optimal E/B mode decomposition using COSEBIs and compressed COSEBIs, Mon. Not. R. Astron. Soc. **464**, 1676 (2017).

[90] A. Lewis and S. Bridle, Cosmological parameters from CMB and other data: A Monte Carlo approach, Phys. Rev. D **66**, 103511 (2002).

[91] A. Lewis, A. Challinor, and A. Lasenby, Efficient computation of CMB anisotropies in closed FRW models, Astrophys. J. **538**, 473 (2000).

[92] A. Gelman and D. Rubin, Inference from iterative simulation using multiple sequences, Stat. Sci. **7**, 457 (1992).

[93] M. B. Gavela, D. Hernandez, L. L. Honorez, O. Mena, and S. Rigolin, Dark coupling, J. Cosmol. Astropart. Phys. 07 (2009) 034.

[94] E. Di Valentino, A. Melchiorri, and O. Mena, Can interacting dark energy solve the H_0 tension?, Phys. Rev. D **96**, 043503 (2017).

[95] E. Aubourg *et al.*, Cosmological implications of baryon acoustic oscillation measurements, Phys. Rev. D **92**, 123516 (2015).

[96] S. Hee, J. A. Vzquez, W. J. Handley, M. P. Hobson, and A. N. Lasenby, Constraining the dark energy equation of state using Bayes theorem and the Kullback-Leibler divergence, Mon. Not. R. Astron. Soc. **466**, 369 (2017).

[97] G. B. Zhao *et al.*, Dynamical dark energy in light of the latest observations, Nature Astron. **1**, 627 (2017).

[98] A. R. Liddle, Information criteria for astrophysical model selection, Mon. Not. R. Astron. Soc. **377**, L74 (2007).

[99] R. E. Kass and A. E. Raftery, Bayes factors, J. Am. Stat. Assoc. **90**, 773 (1995).

[100] A. Heavens, Y. Fantaye, A. Mootoovaloo, H. Eggers, Z. Hosenie, S. Kroon, and E. Sellentin, Marginal likelihoods from Monte Carlo Markov chains, arXiv:1704.03472.

[101] A. Heavens, Y. Fantaye, E. Sellentin, H. Eggers, Z. Hosenie, S. Kroon, and A. Mootoovaloo, No evidence for extensions to the standard cosmological model, Phys. Rev. Lett. **119**, 101301 (2017).